Article

Not peer-reviewed version

Obtaining and Characterization of Hydrogels of Poly (Acid Acrylic-co-Acrylamide) Reinforced with Cellulose nanocrystals from *Acacia farnesiana* L. Willd (Huizache)

Alejandra B Navarro-Hermosillo , Gabriel Landázuri-Gómez , J. Félix Armando Soltero-Martínez , Manuel Alberto Gallardo-Sánchez , Jorge Alberto Cortez-Ortega , Carmen López-López , J. Jesus Vargas-Radillo , José Guillermo Torres-Rendón , Gonzalo Canché-Escamilla , Salvador García-Enriquez * , Emma Rebeca Macias-Balleza *

Posted Date: 4 December 2024

doi: 10.20944/preprints202412.0407.v1

Keywords: Acrylic hydrogels; cellulose nanocrystals; Huizache

 doi:10.20944/preprints202412.0407.v1

Article

Obtaining and Characterization of Hydrogels of Poly (Acid Acrylic-co-Acrylamide) Reinforced with Cellulose nanocrystals from *Acacia farnesiana* L. Willd (Huizache)

Alejandra B Navarro-Hermosillo [1], Gabriel Landázuri-Gómez [1], J. Félix Armando Soltero Martínez [1], Manuel A Gallardo-Sánchez [2], Jorge Alberto Cortez-Ortega [3], Carmen López-López [4], J. Jesús Vargas-Radillo [4], José Guillermo Torres-Rendón [4], Gonzalo Canché-Escamilla [5], Salvador García-Enriquez [4,*] and Emma Rebeca Macias-Balleza [1,*]

[1] Department of Chemical Engineering, University of Guadalajara, Guadalajara 44430, Mexico
[2] Department of Civil Engineering, University of Guadalajara, Guadalajara 44430, Mexico
[3] Department of Chemistry, University of Guadalajara, Guadalajara 44430, Mexico
[4] Department of Wood Cellulose and Paper, University of Guadalajara, Guadalajara 44430, Mexico
[5] Material Unit, Yucatan Center for Scientific Research (CICY), Mérida, Yucatan CP 97205, Mexico
* Correspondence: salvador.genriquez@academicos.udg.mx (S.G.-E.); emma.macias@academicos.udg.mx (E.R.M.-B.).

Abstract: In this work, cellulose nanocrystals (CNC) were obtained from the wood of Acacia farnesiana L. Willd (huizache) by acid hydrolysis. These were used to reinforce polyacrylic acid-co-acrylamide (AAc/AAm) hydrogels synthesized in a solution process by in situ free radical photopolymerization. The nanomaterials were characterized by atomic force microscopy and dynamic light scattering (DLS) and the residual charge on CNC; the nanohydrogels were characterized by infrared spectroscopy, scanning electron microscopy, swelling kinetics, and Young's modulus. The soluble grade cellulose presented 94.6% α-cellulose, 0.5% β-cellulose, and 2.7% γ-cellulose, a viscosity of 8.25 cp, and a degree of polymerization (DP) of 706. The CNC averaged 180 nm in length and 20 nm in width. In the nanohydrogels, it was observed that the Schott kinetic model was followed at times lower than 500 h; after that, the swelling kinetic behavior is linear. The results show that the hydrogel swelling capacity depends on crosslinking agent and CNC concentration as the chemical and morphological CNC properties rather than a CNC source. The presence of CNC decreases the swelling degree compared to hydrogels without CNC. Young's modulus increased with CNC presence and depended on CNC characteristics as crosslinking agent and concentration.

Keywords: Hydrogels; acrylic; nanocrystals of cellulose; Huizache

1. Introduction

Hydrogels are polymeric networks with a three-dimensional configuration that is capable of absorbing large amounts of water or biological solution thanks to hydrophilic groups such as –OH, -COOH, -$CONH_2$, and –SO_3H; while maintaining structural integrity [1]. Due to the ability to mimic many physical properties of tissues, hydrogels are good candidates for multiple biomedical applications, such as cell culture substrates, cell encapsulation, drug delivery, optical and ophthalmological applications, human tissue and duct prosthetics, as well as suture coating and waste treatment [2]. Although most synthetic hydrogels are similar to biological tissue, they are generally fragile and prone to fracture at low strains, which makes their applications difficult where high stress is required [3].

Many strategies have been proposed, including the synthesis of hydrogels using photosensitive initiators, which is a polymerization technique that is usually carried out in short times, can be carried

 doi:10.20944/preprints202412.0407.v1

out at room temperature, does not require organic solvents, and offers dimensional control advantages [4], and above all allows the incorporation of additives or reinforcing agents such as cellulose, which is the most abundant organic substance on planet Earth since it integrates most of the biomass.

Large quantities of agro-industrial waste in Mexico have sparked researchers' interest in alternative ways to use it [5]. *Acacia farnesiana* L. Willd is a plant native to tropical America, known as Huizache, and found from the southern United States to Brazil, Colombia, and Peru. It is popularly called Mimosa farnesiana or white thorn. It is a species with clear potential or future value [6], used for ornamental purposes [7,8]. The leaves, flowers, and fruits are used as fodder for cattle and goats [9–11]. The essential oil of the flowers is used as a flavoring for its pleasant violet aroma. The bark and pods are rich in tannins, so they are used to tan and dye leather [12]. The wood of this species is stiff, so it is used to construct fences and tool handles. It has a high calorific value as a fuel (wood and coal) [13]. Recently, seeds have been studied as a source for the production of biofuels [14], the obtaining of soluble grade cellulose [15], isolation of cellulose nanocrystals [16], phytoremediation of soils contaminated with crude oil [17].

Through different mechanical, chemical, enzymatic, or biological processes, it is possible to obtain cellulose nanofibers and nanocrystals (CNC), which are the most basic structural forms of this polysaccharide and are those that provide considerable improvements in the mechanical properties of the material in which they are present [18–22]. In the 1940s, Rånby first reported that colloidal suspensions of cellulose can be obtained by controlled degradation of cellulose fibers catalyzed by sulfuric acid [23,24]. CNC is a promising renewable nanomaterial with unique properties such as high strength, liquid crystalline behavior, lightweight, biodegradability, and general biocompatibility [25,26]. CNC obtained from various sources by acid hydrolysis have unique characteristics making them suitable for multiples applications. CNC obtained by acid hydrolysis, derived from *Pennisetum purpureum* [27], Eucalyptus kraft pulp [28], Cotton fibers [29], agave bagasse [30], were reported yielding from 1 to 70 %, with sizes ranging from 200 tu up 200 nm and sulfur content between 3-10 mg/g. Bleached pulp fibers were used to produce carboxilated CNC and CNF using maleic acid, enhancing sustainability [31].

These biomaterials are obtained from the acid hydrolysis of wood fiber and plants. They also have excellent properties, are light and flexible, and are obtained from renewable sources in addition to their low cost [32]. These characteristics make nanocrystalline cellulose an interesting option for reinforcing polymeric matrices.

The production of cellulose nanomaterials from lignocellulosic biomass opens an opportunity to develop and apply new materials in nanotechnology [33]. In recent years, cellulose nanomaterial-based hydrogels have emerged as promising materials in the field of biomedical applications due to their low toxicity, biocompatibility, biodegradability, and excellent mechanical stability [34–36]. CNC had been incorporated as fillers to reinforce polymeric hydrogels based on poly(vinyl alcohol) [37–39], Poly(vinyl alcohol)/carboxymethylcellulose [40], α-cyclodextrin [41], polyethylene glycol [42], poly(N -isopropylacrylamide [43–45], polyacrylamide [46–48], Poly(acrylic acid/acrylamide) [49], Polyacrylic acid [50], sodium alginate-g-poly(acrylic acid-co-acrylamide) [51], pectin-Polyacrylic acid [52], carboxymethylcellulose/hydroxyethylcellulose [53], gelatin [54], gelatin/alginate [55], sodium alginate/acrylamide [56], alginate/collagen [57], calcium alginate [58,59], starch [60], pectin [61], collagen [62,63], chitosan [64,65]. In all these systems, improved mechanical properties were observed even at low CNC loadings (generally less than 3 wt%).

The objective of this work is to obtain cellulose nanocrystals from Huizache (*Acacia farnesiana* L. Willd) and apply them as reinforcements in poly (acrylic acid-co-acrylamide) hydrogels (AAc/AAm). We are characterizing them by infrared spectroscopy, swelling kinetics in water, scanning electron microscopy, and rheological properties. Moreover, they were compare with results obtained using CNC from Agave bagasse (*Agave tequilana* Weber var. azul) and commercial CNC from wood.

2. Results and Discussion

2.1. Soluble Grade Pulp Properties

 doi:10.20944/preprints202412.0407.v1

The pulp obtained after hydrolysis and the alkali sulphite-anthraquinone-methanol (ASAM) process yielded of 42% and a Kappa number of 12. In the bleaching process, around 9% of the pulp was lost after cooking, leaving a yield of approximately 33% of soluble grade cellulose from Huizache wood. Lopez (2012) reported yields of 50.1% for a soda process, 47.0% for a Kraft process and 45.3% for a sulfite process for Huizache wood [66].

Other authors have reported similar values using of hardwoods [67,68], or for corn stalks [69]. Dissolving grade pulp has some unique properties and characteristics, including a very high alpha-cellulose content (greater than 90%), a low hemicellulose content (3 to 6%), and traces of lignin and other impurities [70]. Key quality parameters for dissolving grade pulp include alpha cellulose content, alkali solubility, degree of polymerization, molecular weight distribution, and reactivity [71]. The soluble grade cellulose presented 94.6% α-cellulose, 0.5% β-cellulose, and 2.7% Υ-cellulose with 91% whiteness. A viscosity of 8.25 cp and a degree of polymerization (DP) of 706, represents a molecular weight of 241.452 g/mol.-Cellulose materials have DPs that vary depending on the source, production process and treatment [72]. DP values range from 100 to 3000 for commercial celluloses, 20,000 for cotton fiber secondary walls [73].

2.2. Cellulose Nanocrystals Characteristics

Table 1 shows the average results of the hydrodynamic diameter of the CNC obtained by DLS as well as the residual load of acid groups per kg of CNC.

Table 1. The hydrodinamic diameter of CNC obtained by DLS and acid group concentration.

CNC Source	CNC ID	D_H (nm	[AG] (mmol AG/Kg CNC)
Huizache	Hu-A	142	334
	Hu-B	89.5	505
	Hu-C	116	27
	Hu-D	219	216
Agave Bagasse	AB	601	-
Commercial Wood	CW	276	42 (0.4 wt. %)

The CNC were analyzed in an atomic force, and all the samples were homogeneous, with an average length of 180 nm, width of 20 nm, height of 7 nm, and a low dispersion in the size distribution. The dimensions of CNC obtained from wood cellulose are within the range mentioned by other authors [74,75]. In the images of the morphological study of the nanocrystals, CNC with irregular shapes can be seen (Figure 1).

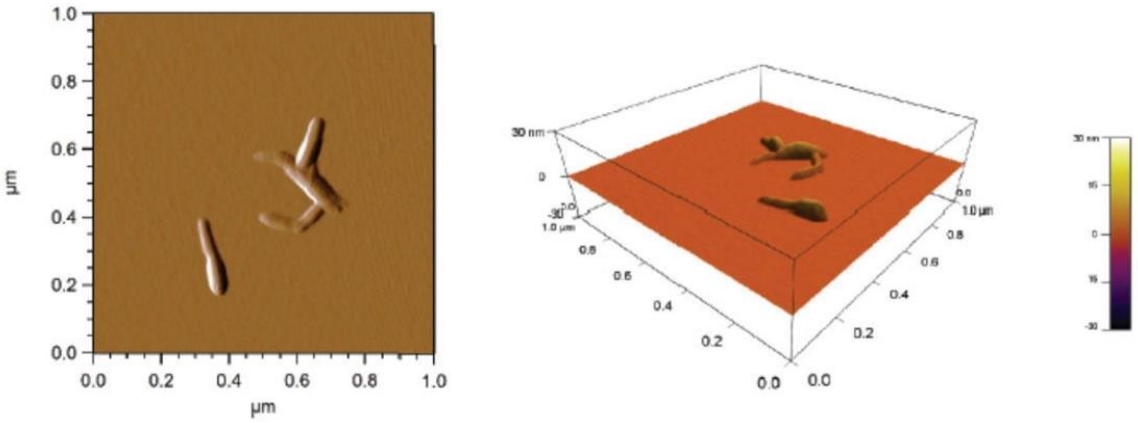

Figure 1. Image of CNC obtained by hydrolysis of α-cellulose from Huizache, with sulfuric acid showing the amplitude and 3D projection technique.

 doi:10.20944/preprints202412.0407.v1

2.3. Hydrogels Characterization

The AAc/AAm hydrogels synthesized after washing presented a reaction yield of 90 ± 2. Before washing they were flexible, after washing and drying they were transparent and hard.

2.3.1. FTIR Spectroscopy of Hydrogels

Figure 2 shows the FTIR spectra of AAc/AAm (50/50) hydrogels crosslinked with n-methylen bis(acrylamide) (NMBA) 0.5 wt. % and photoinitiated, a) without cellulose (control sample), b) with Hu-A CNC 0.1 wt. % and c) Hu-A CNC 1 wt. %. The peaks corresponding to acrylic acid (AAc) can be observed, at approximately 3300 cm^{-1} the band is attributed to the OH groups [76]. The carboxyl group is noticed at 1731 cm^{-1}, and C-O is located at 1169 cm^{-1}, while the C-O and O-H combinations are distinguished at 1421 and 1271 cm^{-1} [4]. The acrylamide (AAm) exhibits the combination of stretching and flexion vibrations of N-H and C-N at 1353 and 670 cm^{-1}, the latter of very low intensity. It can be noticed the presence of the characteristic two bands for amides, Band I, located at 1674 cm^{-1} and Band II at 1588 cm^{-1} attributed to carbonyl stretching and the bending vibrations of N-H bond, respectively, reflecting the presence of amide groups [77,78]. The I and II bands mask the band of combination deformation and stretching vibrations of N-H and C-N at 1615 cm^{-1}. At 2943 y 2883 cm^{-1} are located the bands of CH_2 [4,79]. The stretching vibration bands of N-H for NH_2 are associated with 3342 and 3200 cm^{-1}. The crosslinking agent, NMBA, which has the same functional groups as AAm, exhibits bands at the same wavelengths [79,80]. On the other hand, cellulose exhibits bands attributed to the crystalline structure between 1420 and 1428 cm^{-1} and to the amorphous structure near 900 cm^{-1} (Vârban et al., 2021). The asymmetric and symmetric C-H vibration bands are located at 2943 and 2883 cm^{-1} respectively and overlap with those presented by the hydrogel components. The bands at 1038 cm^{-1}, 1169 and between 3600 and 3200 correspond to the C-O, C-O-C and OH bonds respectively [81–83]. It is also possible to observe characteristic signals of AAc/AAm hydrogel, such as the band that appears around 3450 cm^{-1}, which, according to Orozco-Guareño et al. (2011), is caused by the overlap of the absorption bands of the vibration of the O-H and N-H bonds corresponding to acrylic acid and acrylamide [84]. Asymmetric stretches of the COO- group are also found at 1455 cm^{-1}. A band at approximately 2186 cm^{-1} corresponds to the presence of the C-N bond of AAm and NMBA.

In all cases, the bands observed for cellulose and the crosslinking agent are overlapped by the bands presented by the AAc/AAm hydrogel, making it impossible to determine the interaction of cellulose and the crosslinking agent in the hydrogel.

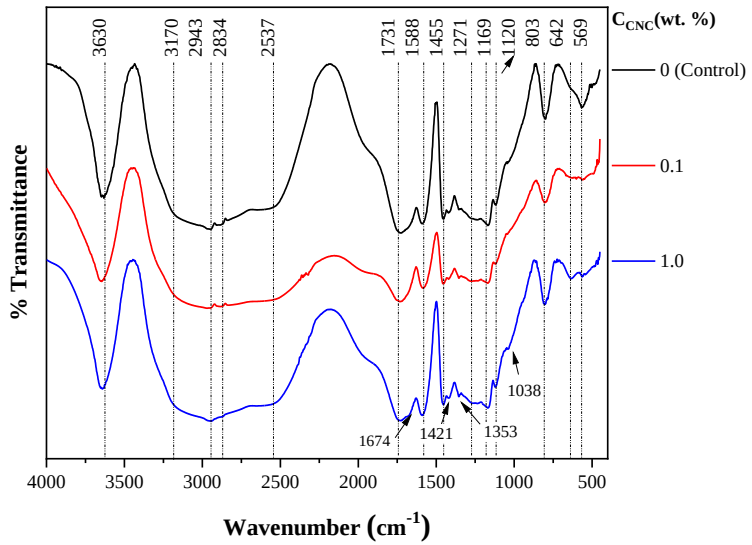

 doi:10.20944/preprints202412.0407.v1

Figure 2. FTIR spectra from AAc/AAm hydrogels with 0.5 wt. % NMBA, for different concentrations of Hu-A CNC (0, 0.1, and 1 wt. %).

Since the FTIR spectra for all hydrogels are similar, whether as a function of NMBA concentration, cellulose concentration, or CNC type, all samples exhibit the same bands at approximately the same wavelengths; qualitatively, no difference could be seen between them that could be attributed to the cross-linking agent or the cellulose, so a more in-depth analysis was carried out.

The areas of all peaks in all spectra were determined by peak deconvolution using Origin software, Version 2021 (OriginLab Corporation, Northampton, MA, USA). The results indicate that for the control samples (hydrogels without cellulose, with NMBA 0.1, 0.5, and 1 wt. %), the percentage of variation in the areas of the peak located at 1731 cm^{-1} is lower than 1 % (0.62 %), and corresponds to the carboxyl of the AAc and which can be considered constant for all formulations since the monomer composition is constant. Thus, the peak areas of all FTIR spectra were normalized with respect to the peak area at 1737 cm^{-1} (A_λ/A_{1731}), this normalization has also been performed for FTIR of acrylic hydrogels [4]. The ratio of A_λ/A_{1731} areas as a function of NMBA concentration for the control samples is shown in Figure 3a for various wavelengths (1169, 1271, 1455, 1588, 1687, 1731 and 2837 cm^{-1}). It can be observed that the area ratio decreases slightly for most of the peaks at the different wavelengths according to power law ($A_\lambda/A_{1731} = a[NMBA]^b$). Still, this ratio shows no dependence on the NMBA concentration for the wavelengths of 1453 and 2837 cm^{-1}, indicating that the bands at these wavelengths are independent of the NMBA concentration. Upon addition of cellulose, the area ratio, A_λ/A_{1731}, of most of the peaks remains constant, as can be seen in Figures 3c and 3d, where the area ratio, A_λ/A_{1731}, is shown for the AAc/AAm hydrogels prepared with Hu-B CNC 0.1 and 1 wt. % , respectively. The symbols represent the experimental data, and the lines represent the power fit ($A_\lambda/A_{1731} = a[NMBA]^b$) of these values. With these results, it is evident that the only area ratio A_λ/A_{1731} dependent of the NMBA concentration is for $\boldsymbol{\lambda}$= 1272 cm^{-1}, where a small increase with the NMBA concentration is observed, (for a better appreciation, a dotted horizontal line was placed as a reference). These results were also observed in Hu-B, Hu-C, and Hu-D cellulose types with CNC 0.1 and 1 wt. %. Figure 3b shows the A_{1272}/A_{1731} area ratio for the four cellulose types, with CNC 0.1 wt. % (Hu-A and Hu-B type) and CNC 1 wt. (Hu-C and Hu-D type) compared to the control samples, in which the A_{1271}/A_{1731} area ratio decreases with increasing NMBA concentration and increases when cellulose is added, this increase being more drastic with CNC 1 wt. % CNC than with CNC 0.1 wt. %. So, from the results shown in Figure 3, it can be said that the bands at 1453 and 2837 cm^{-1} are independent of the NMBA concentration for hydrogels without cellulose, and the band at 1272 cm^{-1} is simultaneously dependent on the NMBA concentration for hydrogels with cellulose, indicating a chemical interaction between cellulose and the AAc/AAm hydrogel because the area ratios decrease with NMBA concentration for control samples, and increase when CNC is added.

 doi:10.20944/preprints202412.0407.v1

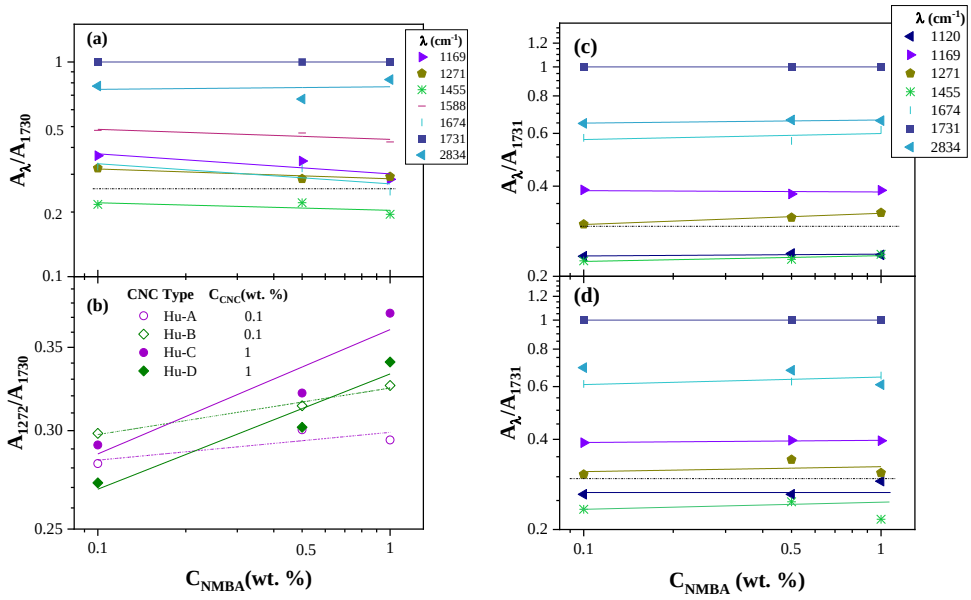

Figure 3. Area relation A_λ/A_{1731} for FTIR spectra of AAc/AAm hydrogels as a function of NMBA concentration a) for Control Samples, b) A_{1272}/A_{1731} for hydrogels containing different type and concentration of CNC, c) and d) A_λ/A_{1731} for hydrogels containing CNC 0.1 and 1 wt. %, respectively.

Now, to relate these results to the chemical composition of the CNC, the value of the ordinate at the origin was taken from the power fit regressions in Figure 3b and 3c for CNC Hu-A type, $(A_\lambda/A_{1731})_0$, and the same was done for the other types of CNCs. The values of $(A_\lambda/A_{1731})_0$, for λ = 1271, 1455 and 1834 cm^{-1}, as a function of the NMBA concentration, for each type of CNC, were graphed as a function of the concentration of acid groups in the nanocrystal (taken from Table 1) and are shown in Figure 4, where it can be observed that (A_λ/A_{1731}) for wavelengths of 1455 and 2834 cm^{-1} decreases with the increase in the degree of cellulose sulfation, while for 1271 cm^{-1} independence from the degree of sulfation is observed. Analyzing each band, the interactions due to the combination of the C-O and O-H bonds at 1271 cm^{-1} of the AAc and dependent on the concentration of the NMBA (Figure 3b, 3c and 3d), it has been reported that the carboxylic groups of the copolymer have complex electrostatic interactions with cationic groups of the acrylic acid during polymerization [85]. While the bands at 1455 and 2834 cm^{-1}, affected by the presence of CNC and mainly attributed to the symmetrical stress and strain vibrations of CH_2 respectively [76], decrease with increasing concentration of sulfate groups, the band at 1455 also overlap with asymmetric stretches of the COO^- group. Then, the chemical interaction of cellulose with the hydrogel decreases as the degree of sulfation increases, i.e. the decrease of OH groups on carbon 6 of cellulose. The above suggests that the chemical interaction takes place between the OH groups of cellulose and the acidic monomer. It has been reported that acrylic acid and cellulose exhibit chemical interactions at 1651, 1450, and 1170 cm^{-1} [86].

Preprints.org (www.preprints.org) | NOT PEER-REVIEWED | Posted: 4 December 2024 doi:10.20944/preprints202412.0407.v1

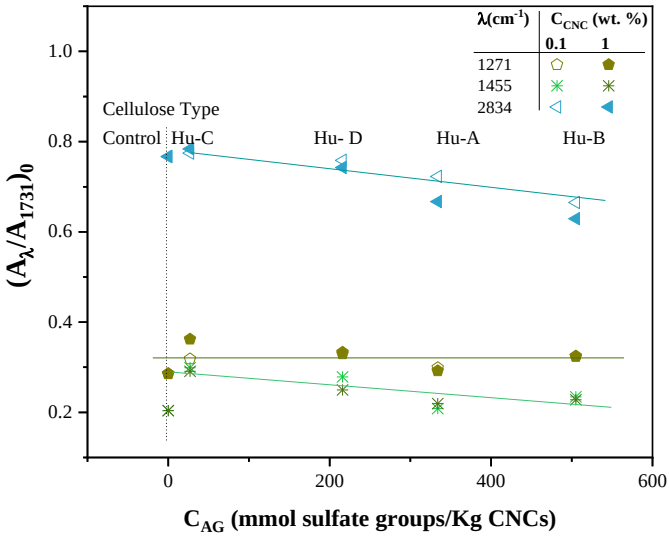

Figure 4. $(A_\lambda/A_{1731})_0$ as a function of the C_{AG} in CNC for λ = 1271, 1455, and 2834 cm^{-1} and for the diffetent CNC types.

2.3.2. Hydrogels Swelling Kinetic

The effect of NMBA concentration (0.1, 0.5, and 1 wt. %) on the swelling kinetics for AAm/AAc (50/50) hydrogels as a function of CNC concentration (0.1 and 1 wt. %) from Huizache with different hydrolysis conditions (Hu-A, Hu-B, Hu-C, and Hu-D treatments), can be observed in Figures 5A to 5D respectively. The symbols represent the experimental data, while the lines correspond to the second-order kinetic model proposed by Schott [87], whose parameters are reported in Table 2. The experimental data and the Shoot equation parameters are the average of five determinations. Figure 5A shows the swelling kinetics as a function of Hu-A type CNC content and NMBA concentration: (a) 0.1, (b) 0.5, and, (c) 1. wt. %; it is evident that most of the samples reached equilibrium within 100 h, however, the kinetics were followed up to 10 days, it can be noted that the amount of water absorbed by the hydrogel decreases for both hydrogels with CNC 0.1% and 1 % compared to the control sample (without CNC), this occurs for the three NMBA concentrations used (0.1, 0.5, and 1 wt. %) and is shown in (a), (b) and (c) of Figure 5A. This effect is probably because the crosslinking density increases with the concentration of CNC since it acts as a crosslinking agent, hindering water absorption [88]. This phenomenon has also been observed by Lim et al., (2017), when using cellulose nanocrystals as a reinforcing material in poly(acrylic acid)-based hydrogels with 5, 10, 15, 20, and 25% by weight of CNC, their results show a higher degree of swelling in hydrogels with 5% w/w of nanocrystalline cellulose, while the incorporation of more than 5% w/w tended to decrease the swelling ratio, they attribute this behavior to the increase in hydrophilic hydroxyl groups, which facilitate the absorption of water within the hydrogel [89]. The decrease in swelling concerning the CNC content is dependent when C_{NMBA} is 0.1%; however, for C_{NMBA} 0.5 and 1 wt. % no considerable changes are observed concerning the CNC content. In hydrogels based in sodium acrylate and N-acrilamide [90], 2-hydroxiethylmethacrylate [90], and NIPAM [91], increasing the cross-link concentration reduces the equilibrium degree of swelling.

 doi:10.20944/preprints202412.0407.v1

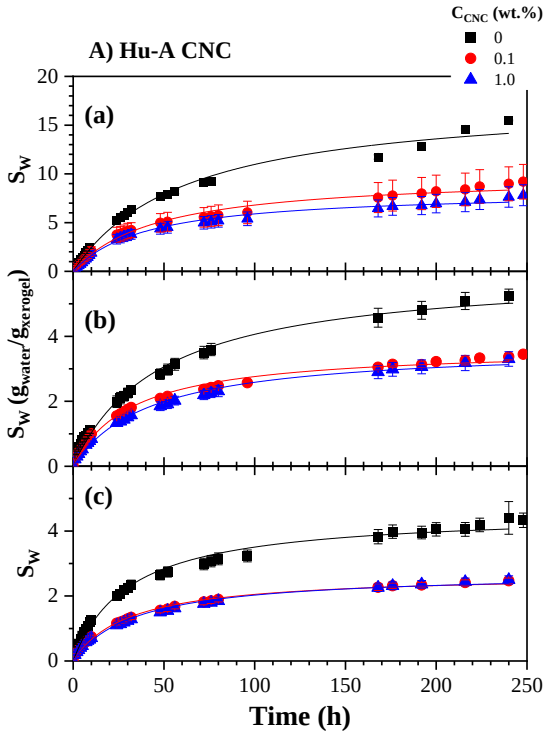

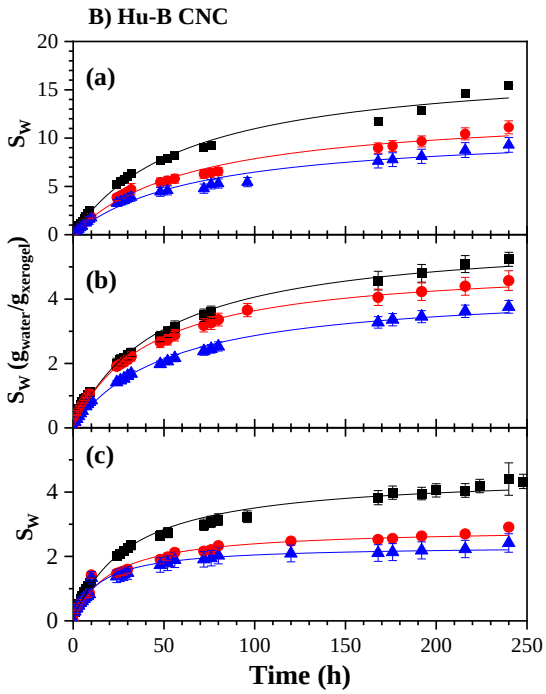

 doi:10.20944/preprints202412.0407.v1

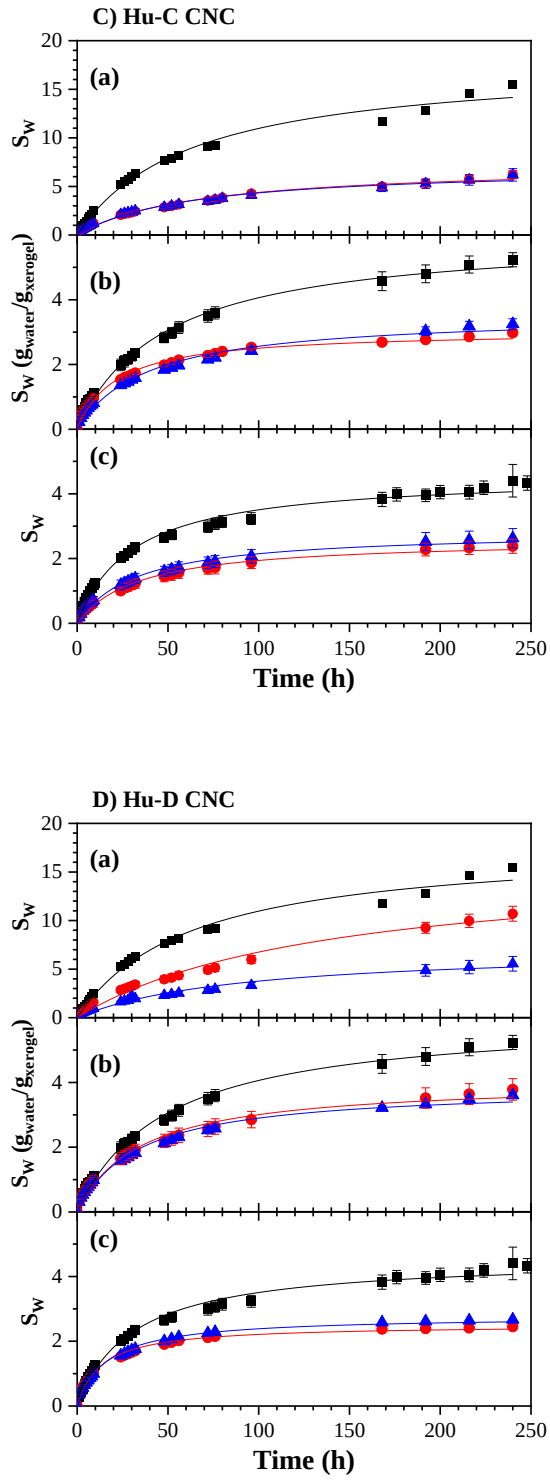

Figure 5. Kinetic swelling of AAc/AAm hydrogels with different types of CNC; A) Hu-A, B) Hu-B, C) Hu-C, and D) Hu-D and concentrations (0, 0.1 and 1 wt. %) and for different NMBA concentrations a) 0.1, b) 0.5, and c) 1wt. %.

 doi:10.20944/preprints202412.0407.v1

Table 2. Schoot equation parameter for swelling kinetic of AAc/AAm hydrogels as a function of NMBA and CNC concentration, as for CNC type.

CNC Concentration (wt. %)			0.1			1.0		
CNC Source	CNC ID	[NMBA] Shcott (wt.%) Eq. parameters	0.1	0.5	1	0.1	0.5	1
Control Sample (without CNC)		$S_{w\infty}$	8.12 ± 1.03	4.79 ± 0.14	4.64 ± 0.31	8.12 ± 1.03	4.79 ± 0.14	4.64 ± 0.31
		$Kx10^3$	2.9 ± 0.3	5.8 ± 0.27	6.97 ± 0.16	2.9 ± 0.3	5.8 ± 0.27	6.97 ± 0.16
		R^2	0.9833 ± 0.0033	0.9884 ± 0.0032	0.9870 ± 0.0063	0.9833 ± 0.0033	0.9884 ± 0.0032	0.9870 ± 0.0063
Huizache	Hu-A	$S_{w\infty}$	10.2 ± 2.13	3.70± 0.12	2.71 ± 0.13	8.46 ± 1.19	3.77 ± 0.27	2.77 ± 0.14
		$Kx10^3$	2.1 ± 0.6	8.1 ± 0.5	11.2 ± 2	2.85 ± 0.5	5.95 ± 0.5	10 ± 0.5
		R^2	0.9868 ± 0.0015	0.9906 ± 0.0010	0.9909 ± 0.0031	0.9908 ± 0.0034	0.9879 ± 0.0026	0.9872 ± 0.0021
	Hu-B	$S_{w\infty}$	13.8 ± 0.96	4.45 ± 0.29	2.89 ± 0.07	11.54 ± 0.92	5.24 ± 0.38	2.38 ± 0.25
		$Kx10^3$	1 ± 0.2	4.2 ± 0.6	17 ± 2.5	1.15 ± 0.14	4.5 ± 0.7	28 ± 2
		R^2	0.9857 ± 0.0035	0.9900 ± 0.0020	0.9779 ± 0.0023	0.9755 ± 0.0021	0.9924 ± 0.0015	0.9753 ± 0.0043
	Hu-C	$S_{w\infty}$	7.79 ± 0.62	3.11 ± 0.10	2.66 ± 0.18	7.61 ± 0.93	3.70 ± 0.22	2.91 ± 0.98
		$Kx10^3$	1.7 ± 0.3	14 ± 0.9	11.1 ± 3	1.9 ± 0.4	6.5 ± 1	10 ± 1
		R^2	0.9786 ± 0.0027	0.9844 ± 0.0022	0.9838 ± 0.0098	0.9756 ± 0.0020	0.9782 ± 0.009	0.9846 ± 0.0098
	Hu-D	$S_{w\infty}$	7.82 ± 1.95	4.19 ± 0.33	2.52 ± 0.07	17.2 ± 1.4	3.99 ± 0.96	2.79 ± 0.10
		$Kx10^3$	1.5 ± 0.7	6.4± 0.9	29 ± 4	0.39 ± 0.007	7.1 ± 0.9	21.6 ± 1.9
		R^2	0.9657 ± 0.0203	0.9788 ± 0.0072	0.9884 ± 0.0016	0.9814 ± 0.0032	0.9802 ± 0.0022	0.9898 ± 0.0020
Agave Bagasse	AB	$S_{w\infty}$		5.95 ± 0.41			4.54 ± 0.35	
		$Kx10^3$		4 ± 0.4			6.5 ± 0.7	
		R^2		0.9724 ± 0.0076			0.9900 ± 0.0032	
Commercial Wood	CW	$S_{w\infty}$		4.35 ± 0.33			3.61 ± 0.31	
		$Kx10^3$		4.1 ± 0.09			9.1 ± 1	
		R^2		0.9913 ± 0.0022			0.9911 ± 0.0041	

* Sw_∞ in $g_{water}/g_{xerogel}$ and K in (h^{-1}).

When CNC Hu-D type is used, results are similar to those exhibited with Hu-A type cellulose (Figure 5D). In contrast, whit the Hu-C cellulose type (Figure 5C), there are no considerable changes with respect to the cellulose content for the three NMBA concentrations, even with 0.5 and 1 wt. % NMBA, there is a lower degree of swelling with 0.1 % CNC than with 1 % CNC (Figures 5C(b) and 5C(c)). In change, for Hu-B type cellulose, Figure 5B, the hydrogel swelling gradually decreases with cellulose concentration for the three NMBA concentrations. A potential reason for these behaviors can be attributed to the degree of cellulose sulfation; analyzing the two extremes, samples Hu-B and Hu-C, whose acid group concentration are 505 and 27 mmol/Kg cellulose, respectively. It is noted that when the concentration of acid groups is low, the interactions between the CNC and the hydrogel

 doi:10.20944/preprints202412.0407.v1

are greater than when the concentration of acid groups is high (See Figure 4), in other words, there is more significant than degree of crosslinking between the lower the degree of sulfation and therefore a lower degree of hydration of the hydrogel, that is why the hydrogels synthesized with Hu-C type CNC (Figure 5C) present a lower degree of hydration and this is independent of the cellulose concentration. Nevertheless, the hydrogels synthesized with Hu-B type CNC (Figure 5B), with a high degree of sulfation and, therefore, a low level of crosslinking, exhibit a degree of hydration dependent on the CNC concentration. The hydrogels with Hu-A and Hu-C, whose acid group concentrations are 334 and 216, respectively, only exhibit concentration dependence at low NMBA concentrations (Figures 5A and 5C). The acid groups influence and enhance the swelling kintetics because the interplay of osmotic presure as the ionic interactios [92], and a decrease in pH reduce the swelling due to the acidic groups transform to undisssociated forms itself [92,93].

Table 2 shows the Shoot equations parameters [87] for the AAc/Aam hydrogels swelling kinetic as a function of CNC type and concentration and NMBA concentration; each value corresponds to an average of five experiments fit, the fit for the experimental data average is similar to the average of five fits. Table 2 shows that the swelling capacity diminishes with NMBA concentration for the control sample and for AAm/AAc hydrogels reinforced with CNC 0.1 and 1 wt. %; while the K value increases with CNC concentration only for NMBA 0.1 wt. % and for NMBA 0.5 and 1 wt. % decreases for most samples or remains at similar valor, considering the standard deviation. As in Figure 5, SW_∞ achieves similar valor for 1 wt. % of NMBA, independent of Huizache CNC concentration (2.70 ± 0.18), for NMBA 0.5 wt. %, excluding Hu-B, the average value is 3.74 ± 0.36. The CNC type AB and CW values are higher than those obtained for Huizache. The comparison of CNC sources on swelling kinetic is shown in Figure 6.

Figure 6 shows the swelling kinetics for AAc/AAm hydrogels with 0.5% NMBA, for different CNC concentrations: a) 0.1 and b) 1 wt. %, and for various types of CNC: from Huizache at different hydrolysis conditions (Hu-A to Hu-D), from agave bagasse (AB) and commercial CNCs from wood (CW). In all cases, the degree of swelling, Sw, is lower for hydrogels with CNC than without CNC. However, differences are observed with respect to the CNC content, while for 0.1 wt. % CNC (Figure 6a), the sample containing CW does not show any difference with respect to the control sample, the other samples show a lower magnitude in the degree of swelling, with the hydrogel with CNC type Hu-C showing a lower degree of swelling and the Hu-B sample showing a higher degree of swelling. When 1% CNC is added (Figure 6b), most hydrogels present a swelling degree between 2.5 and 3 while the sample with CB exhibits a higher swelling degree (3.5). In both cases, the sample with CB exhibits a higher swelling degree than those in which Huizache or agave bagasse CNC were used. This behavior may be attributed to the nanocrystal size, which is 4 to 7 times larger than other formulations.

On the other hand, the difference between all types of cellulose can be attributed to the degree of sulfation of the CNC, so Figure 6c shows the equilibrium swelling Sw,∞, obtained from the adjustments to the second-order Schott model [87], as a function of the concentration of acid groups (from Table 1) for the different types of CNC. It can be observed that for NMBA concentrations of 0.1 and 0.5 wt. %, the degree of swelling increases with the degree of sulfation, i.e., the greater the swelling, the lower the degree of cross-linking, which suggests that by increasing the concentration of sulfate groups, the concentration of OH at cellulose carbon 6 is reduced, and therefore the interaction sites between cellulose and hydrogel, which FTIR also confirmed. On the other hand, with 1 wt. % NMBA, the lowest degrees of swelling are observed regardless of the amount of cellulose, while for CNC, 0.1 wt. %, $S,w\infty$ remains almost invariable with C_{AG}, with 1 wt. % a decrease in the degree of swelling is observed. This behavior may indicate that CNC also acts as a crosslinking agent at these CNC concentrations. Finally, the effect of CNC size on the swelling degree is shown in Figure 6d, where Sw is also observed depending on the CNC concentration, the swelling degree decreases with the nanocrystal length (denoted by the solid line), perhaps because once cellulose has interacted with the polymer, increasing the nanocrystal length increases the possible interactions between them, while for CNC 1 wt. %, the swelling degree increases for sizes greater than 100 nm. Thus, there is a dependence between the degree of swelling of the hydrogel and the concentration and length of CNC.

Preprints.org (www.preprints.org) | NOT PEER-REVIEWED | Posted: 4 December 2024 doi:10.20944/preprints202412.0407.v1

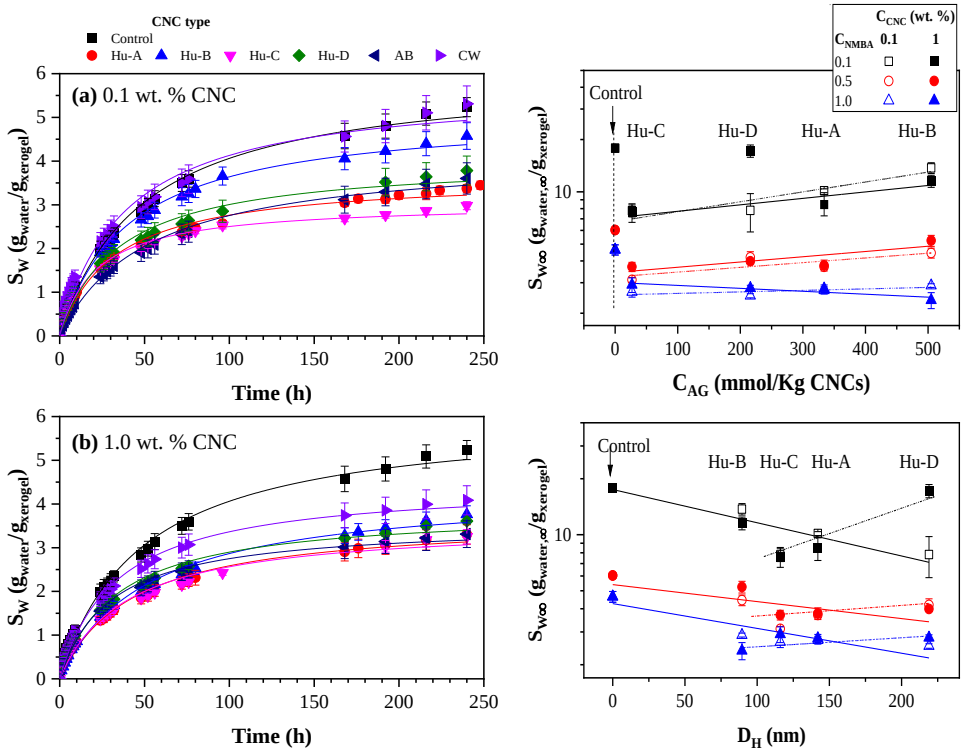

Figure 6. Effect of the type of CNC on the swelling kinetics with CNC a) 0.1 and, b) 1 wt. % and NMBA 0.5 wt. %. Dependence of Sw∞ on c) acid group concentration on cellulose and d) CNC hydrodinaic diameter.

According to Işık, in the case of acrylic acid-rich hydrogels, the swelling capacity is possibly controlled by the acrylic acid portion in the copolymer [94]. This behavior is probably attributed to the intermolecular hydrogen bonds between carboxylic acids and amide groups and the intramolecular hydrogen interactions between amide groups. Those results lead us to infer that the nature of the crosslinking agent strongly impacts the hydrogels' absorption properties, even though the monomers and their ratio are similar. In the AAc/AAm hydrogel reported in the present work, a pseudo-equilibrium was reached at approximately 100 h. Since the hydrogels continued to absorb water very slowly, they were measured for a more extended period of 10 days, and the results presented in Figures 5 and 6 were obtained. However, water uptake continued to increase slightly and was monitored until 2000 h. Figure 7 shows the swelling kinetics for AAm/AAc hydrogels with 0.1, 0.5, and 1 wt. % NMBA at 500 h with (a) 0.1 and (b) 1 wt. % Hu-C type CNC, and at 2000 h with (c) 0.1 and (d) wt. % Hu-C type CNC. At 500 hours. The symbols represent the experimental data, and the lines correspond to the Schott model [87]. In Figures 7a and 7b, the samples with 0.1 and 1 % cellulose reach a steady state at approximately 100 h; as can also be seen in Figure 5, those steady states are not prolonged for the samples without CNC, nor for the sample with 0.1 wt. % NMBA and 0.1 % CNC, it is evident that after 240 hours, there is a new increase in the swelling. Figures 7c and 7d show swelling kinetics up to 2000 h. Evidently, after 500 h, the swelling increases linearly with time without reaching a new steady state. This behavior occurs in all hydrogels, both without cellulose and with cellulose, and for all NMBA concentrations. The lines correspond to a linear regression, and the slopes are shown in Table 3. This slope represents the hydrogel swelling rate at a significant or very long time, while all the lines start at the origin.

 doi:10.20944/preprints202412.0407.v1

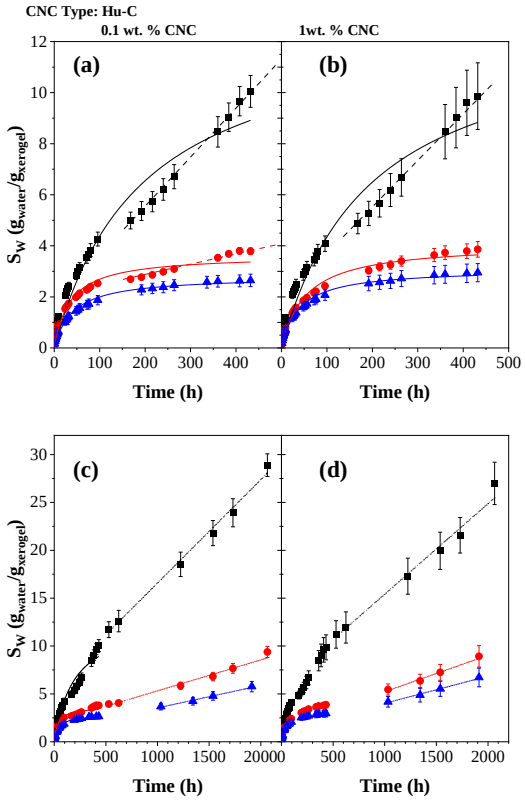

Figure 7. Swelling kinetics of hydrogels with CNC type Hu-C at 500 h with a) 0.1 and b) 1 wt. % of CNC and at 2000 h, also with 0.1 and 1 CNC wt. % (c) and (d) respectively.

Table 3. Line equation parameter for swelling kinetic of AAc/AAm hydrogels as a function of NMBA and CNC concentration, as for CNC type.

CNC Concentration (wt. %)			0.1			1.0		
CNC Source	CNC ID	[NMBA] / slope (wt.%) / Lineal Eq'n	0.1	0.5	1	0.1	0.5	1
Control Sample (without CNC)		m	14.03 ±2.17	3.79 ± 0.60	4.46 ± 0.33	14.03 ±2.17	3.79 ± 0.60	4.46 ± 0.33
		R^2	0.96182	0.99964	0.98217	0.96182	0.99964	0.98217
Huizache	Hu-A	m	7.27 ± 0.44	5.37 ± 0.31	2.82 ± 0.20	2.41 ± 0.44	1.86 ± 0.06	1.85 ± 0.06
		R^2	0.98664	0.99374	0.99167	0.98471	0.99219	0.99394
	Hu-B	m	9.98 ± 0.29	3.97 ± 0.14	2.24 ± 0.07	7.48 ± 0.18	2.56 ± 0.89	1.71 ± 0.13
		R^2	0.99381	0.99312	0.99218	0.99695	0.99618	0.9734
	Hu-C	m	5.50 ± 0.27	2.38 ± 0.16	1.79 ± 0.09	5.84 ± 0.29	2.47 ± 0.17	1.91 ± 0.11
		R^2	0.99356	0.9748	0.98731	0.9909	0.9832	0.98667
	Hu-D	m	8.79 ± 0.33	2.91 ± 0.17	2.12 ± 0.13	3.89 ± 0.28	2.80 ± 0.13	2.34 ± 0.13
		R^2	0.9963	0.98686	0.95481	0.99322	0.999449	0.95943
Agave Bagasse	AB	m		4.46 ± 0.09			3.42 ± 0.06	
		R^2		0.98823			0.98927	

 doi:10.20944/preprints202412.0407.v1

Commercial Wood	**CW**	**m**	2.96 ± 0.07	2.76 ± 0.05
		R^2	0.98669	0.98696

For $S_W = b + mt$, m is in $g_{water}/g_{xerogel}$ h^{-1} and b value is 0.005 ± 0.004.

Orozco-Guareño et al. (2011) established that different behaviors can be observed depending on the degree of crosslinking and the presence (or absence) of specific interactions between comonomers in the copolymer chain [84]. As shown in Table 2, the slope diminishes with NMBA and CNC concentration, and the CNC characteristics play an important role in swelling behavior.

2.3.3. Hydrogels Morphology by SEM

Porosity in this type of material is essential as it can determine the water and ion absorption capacities. Figure 8 shows micrographs of hydrogels with 3 (a,b,c) and 8 (d) hours of swelling at magnifications of 50x, 1kx, and 5kx for hydrogels with different concentrations of Hu-C and NMBA. The images on the left (50x) show the hydrogels obtained once swollen, frozen, fractured, and freeze-dried; porous solids can be observed in all cases. Figure 8a.2 shows the image received for the control sample, with 0.1 wt. % NMBA, pores between 5 and 20 mm can be noticed, and the topology of the hydrogel is seen with tiny pores and distributed in a non-uniform manner. When zooming in (Figure 8.a.3), a non-homogenous distribution of pores can be noticed, with sizes between 1 and 5mm and small protuberances distributed randomly on the pore walls. Figure 8b.2 presents the images of hydrogels with Hu-C type CNC (0.1 wt. %). A structured material with pores between approximately 10 and 20 mm can be distinguished when increasing the magnification to 5 kx (Image 8b.3), and the hydrogel walls present elongated and thin bumps, giving a "chicken skin" appearance. By increasing the amount of CNC and NMBA, (Image 8c.2), the pore size decreases with the concentration of CNC and NMBA (5-10 mm), attributed to a lower degree of swelling and a higher level of crosslinking. In 8c.2 it is noticeable that the walls of the hydrogel are not entirely smooth and small protuberances are observed. In images 8d, micrographs are shown for a hydrogel with a longer hydration time; a better definition of pores is evident with a non-uniform size distribution and smoother walls than a lower degree of swelling (8b).

The morphology of collagen hydrogels reinforced with CNC is reported by Li et al. (2023) for vast quantities of CNC (5-20 wt. %), compared to our research. At low CNC concentration, 5 and 10 wt. %, they found interconnected porous structures with pores inside, at higher concentrations, 15-20 wt. %, the hydrogel is more compact, the porosity decreases, and the surface is smoother [95].

Wong et al. (2015) synthesized polyethylene oxide hydrogel films for various crosslinking agent concentrations [96]. They studied swelling kinetics and mechanical properties and presented a very detailed morphology analysis by SEM. The images are similar to those obtained in our research (Figures 8a to 8c). They describe hydrogel as a mesh structure with interconnected micropores, empathizing that the equilibrium is achieved in only five hours because the channels can transport water. They determined that the mesh size diminishes with crosslinking concentrations, and the values go from 10.7 to 1.6 nm. Xion et al. (2014) reported morphology for superabsorbent polymers as a fucntion of the type or cross-linker agent and the images exhibited porous architecture with different porous size and size distribution due to the crosslinker functional groups, distance between bonds and steric effects [97]. Their images are similar to those in Figures 8c. The morphology of collagen hydrogels reinforced with CNC is reported by Li et al. (Li et al., 2023) for vast quantities of CNC (5-20 wt. %), compared to our research. At low CNC concentration, 5 and 10 wt. %, they found interconected porous structures with pores inside, at higher concentrations, 15-20 wt. %, the hydrogel is more compact, the porosity decreased, and, the surface is smoother.

 doi:10.20944/preprints202412.0407.v1

a) Control, NMBA: 0.1 wt. %

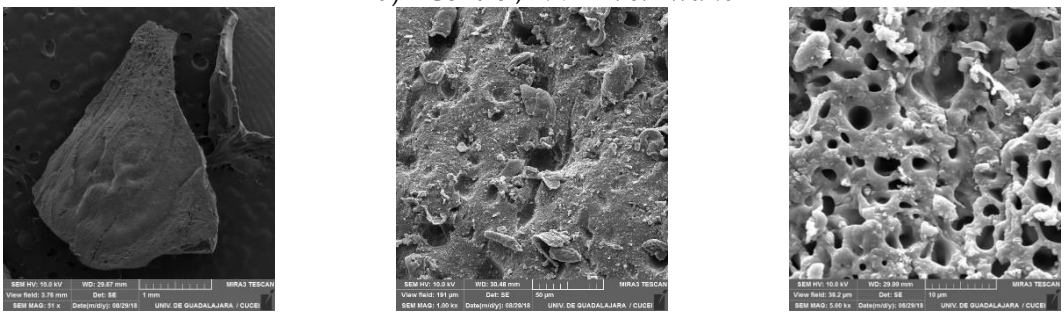

b) Hu-C CNC: 0.1 wt. %, NMBA: 0.1 wt. %

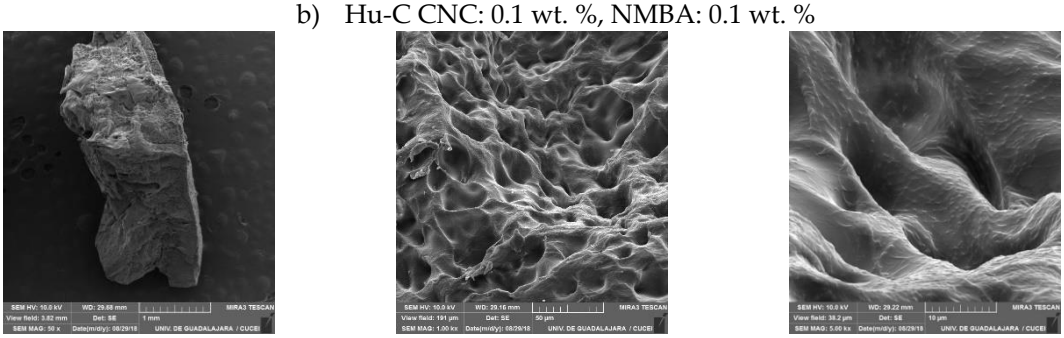

c) Hu-C CNC: 1 wt. %, NMBA: 0.5 wt. %

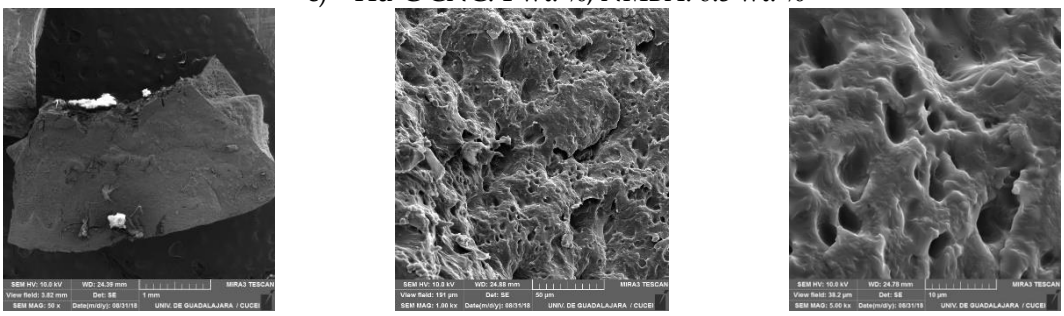

d) Hu-C CNC: 0.1 wt. %, NMBA: 0.1 wt. %

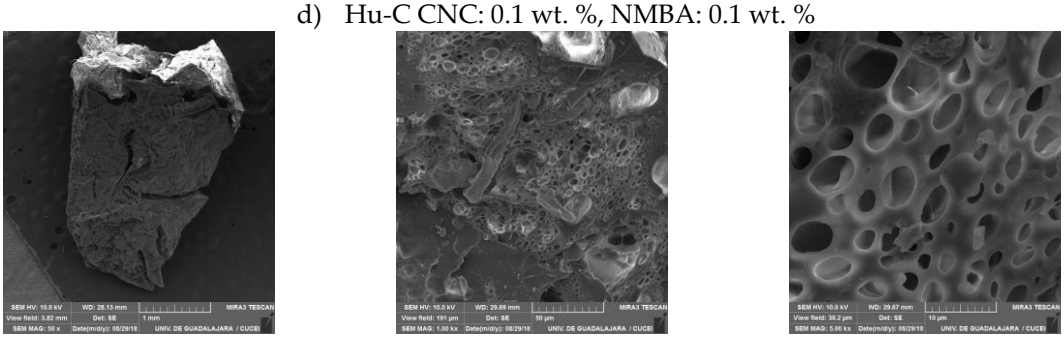

Figure 8. SEM image for AAc/AAM hydrogels a) for control sample at 0.5 wt. % NMBA and 3 hours of hydration, and at different CNC and NMBA concentrations and swelling times, b) CNC 0.1 wt. %, NMBA 0.1 wt. % and swelling time of 3 h, c) CNC 1 wt. % CNC, NMBA 0.5 wt. % and swelling time of 3 h and d) 0.1 wt. % CNC, 0.1 wt. % NMBA and swelling time of 8 h.

Figure 9 shows the SEM images for hydrogels swollen at equilibrium (72 hours), or in our case, at pseudo-steady state, for hydrogels with 0.5 wt. % NMBA and 0.1 wt. % CNC type: a) Hu-A, and b) Hu-B. In the images on the left, the complete samples are shown, and unlike the images obtained a few hours after swelling (Figure 8), the pores can be observed at 17 and 34 x, respectively, it is also evident that in sample A, with a higher degree of crosslinking and lower degree of swelling than sample B (Figure 6a), pores between 0.1 and 1 mm are observed. In the close-up, it is evident that the walls of the pores are smoother than those observed at low swelling times, while the sample with Hu-B CNC, which swells more, when freeze-dried, no longer has the appearance of a porous solid, but instead looks like long lamellae whose walls have smooth and rough areas randomly distributed (9.2.a), when magnifying the rough part curved grooved textures can be observed (Figure 9.b.2).

 doi:10.20944/preprints202412.0407.v1

a) Hu-A CNC: 0.1 wt. %, NMBA: 0.5 wt. %

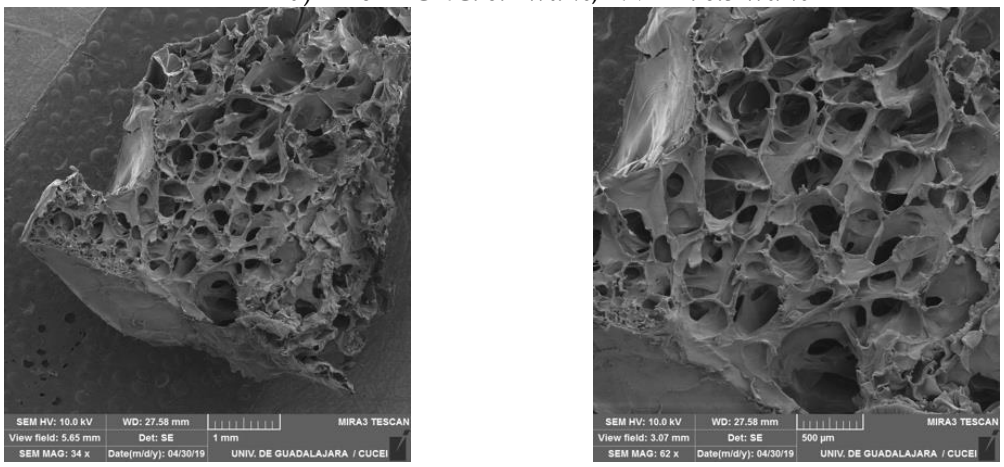

b) Hu-A CNC: 0.1 wt. %, NMBA: 0.5 wt. %

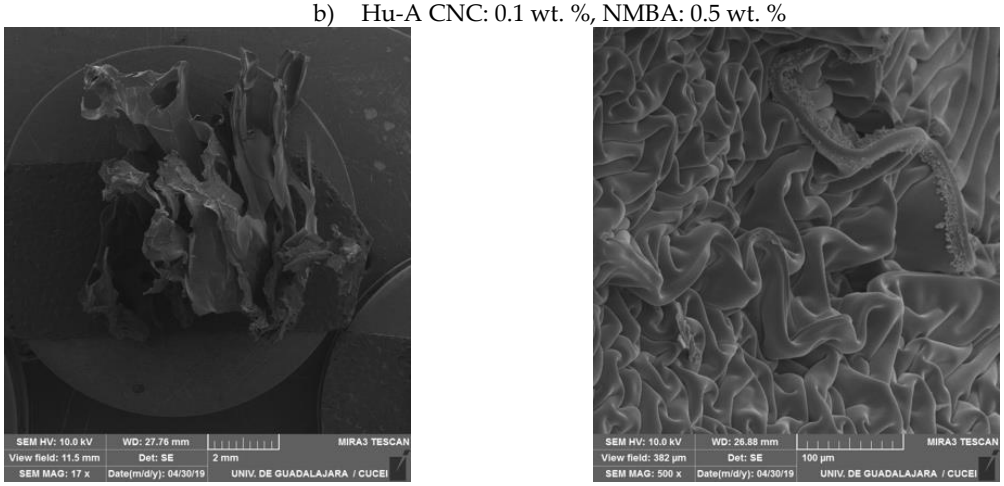

Figure 9. SEM image for AAc/AAM hydrogels with 0.1 wt. % CNC and 0.5 wt. % NMBA for different type of CNC a) Hu-A Type, b) Hu-B Type.

2.3.4. Hydrogels Rheological Characterization

Young's modulus and compression tests (squeeze) were performed to obtain the hydrogels' mechanical properties. The effect of NMBA at a constant concentration of 1 wt% Hu-C CNC at 300 h of swelling is shown in Figure 10a, and it can be observed that a higher concentration of NMBA results in an increase in the slope of the graph, i.e., in Young's modulus. This result may be because the strength of the material increases dramatically with increasing crosslinking density. It has been shown that adding more crosslinking agents can easily increase the swelling capacity. A wide range of studies have been carried out on the dependence of mechanical properties on the concentration of the crosslinking agent in hydrogels [98]. The effect of the amount of CNC on the equilibrium properties of hydrogels is shown in Figure 10b. and it can be observed that as the amount of CNC in the hydrogel increases, the Young's modulus increases, indicating that the CNC acts as a reinforcing material.

 doi:10.20944/preprints202412.0407.v1

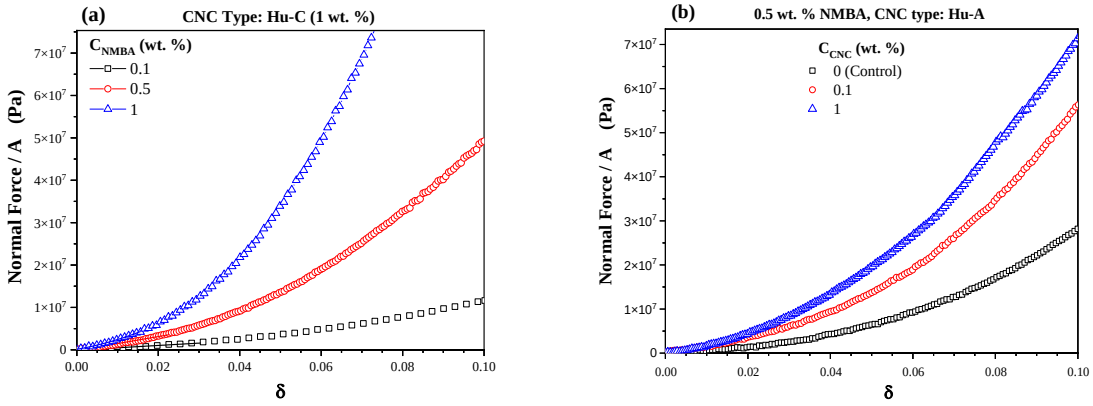

Figure 10. Effect of NMBA and CNC on Young's modulus of type C CNC.

Figure 11 shows the response surface of Young's modulus as a function of NMBA concentration and equilibrium swelling degree ($S_{W\infty}$) for hydrogels with 0.1 and 1 wt. % cellulose, swollen a) 300 h and b) 2000 h. At 300 h and 0.1 wt. % CNC (Figure 11a), it can be seen that Young's modulus increases with NMBA concentration and decreases with a swelling degree. However, at low NMBA concentrations, a slight increase is observed, which is lower than the variation in the results (See Table 4). It is expected that the greater the amount of CNC, the Young's modulus will increase, but this is only true for swellings less than 10, for higher $S_{W\infty}$, two behaviors occur: at low concentrations of NMBA, the reinforcing effect of CNC is enhanced, while at high concentrations of NMBA, the Young's modulus decreases drastically. It has been reported that for composite materials, there is a concentration above which the properties are reduced with the concentration of the composite; in this case, the combination of the concentration of crosslinking agent and reinforcing material produces the same effect. The cross-linkers modifies the hydrogel mechanical properties by interactions polymer networks [99], based on a tetrafuncional cross-linker (ethylene dimethacrylate) and poly(ethylene grlycol, the system exhibithed significant differences in swelling and mechanical properties concerning their nature and concentration [100]. At 2000 h of swelling, Young's modulus in the hydrogels shows the same trend (Figure 11b); it can be observed that regardless of the CNC concentration, the modulus increases with the NMBA concentration, the improvement in the mechanical properties is also observed for 1 wt. % of CNC at low crosslinker concentrations and for 0.1 wt. % at high crosslinker concentrations. Adding CNC to PVA hydrogels enhances the mechanical strength in 303 % at a deformation of 60 % [101], besides, anionic and cationic CNC form hydrogen bonds which improve the hydrogel stability and strength [102]. Tables 5 and 5 show the Young's modulus for hydrogel as a function of NMBA concentration and CNC source and concentration at swelling times of 300 and 2000 hours, respectively. The Young's modulus increases with NMBA and CNC concentration and diminishes with swelling time.

Figure 11c and 11d show the morphological and chemical properties of the CNC in the Young's modulus, such as the hydrodynamic radius and the concentration of acidic groups at 300 and 2000 h of swelling. For 1% CNC, it is observed that the Young's modulus generally increases with the CNC length, both at 300 and 2000 h, except for long lengths and low C_{AG} at 2000 h, as can be seen in Figure 12b. The loss of mechanical properties due to swelling time, i.e. at higher swellings, is shown by comparing 1% CNC at 300 and 2000 h (Figure 11c and 11d respectively), in which this loss is more significant for long CNC lengths and low C_{AG}. For 0.1% CNC, the dependence of the Young's modulus on the CNC characteristics becomes more complex; at 300 h, the Young's modulus increases, with respect to that obtained with 1% CNC, at short lengths and high C_{AG}. At 2000 h, the loss of properties is evident more noticeable at the response surface extremes.

Preprints.org (www.preprints.org) | NOT PEER-REVIEWED | Posted: 4 December 2024 doi:10.20944/preprints202412.0407.v1

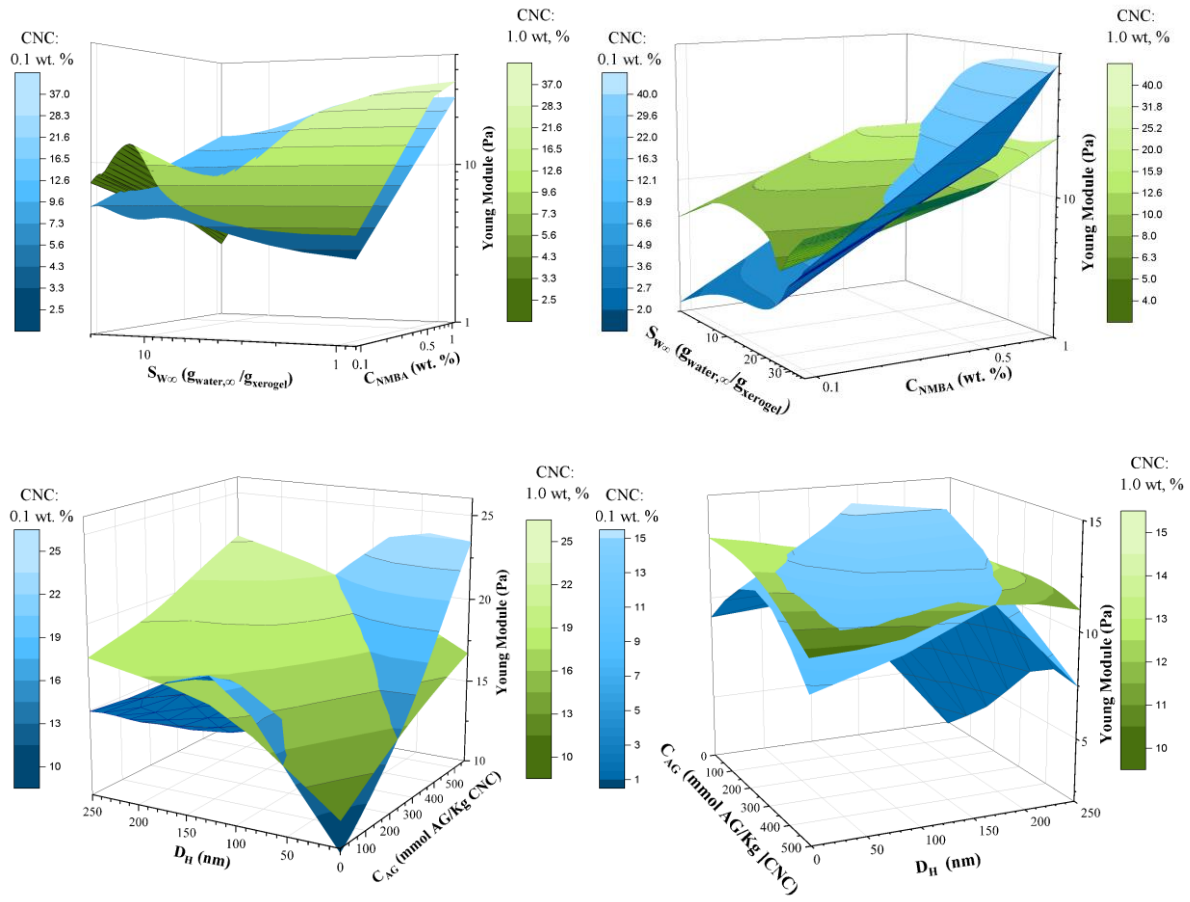

Figure 11. Response surface of Young's modulus of AAc/AAM hydrogels as a function of NMBA concentratión and hydrogelo swelling at a) 300 h, b) 2000 h and as a function of CNC characteristics (D_H and C_{AG}) at b) 300 h, and d) 2000 h.

Table 4. Young Modulus of AAc/AAm hydrogels as a function of CNC type and concentration, and NMBA concentration at 300 h of swelling.

C_{CNC} (wt. %)		0.1			1		
CNC Type	C_{NMBA} (wt. %)	0.1	0.5	1	0.1	0.5	1
Control		9.7 ± 1.8	10.5 ± 6.2	17.5 ± 7.2	9.7 ± 1.8	10.5 ± 6.2	17.5 ± 7.2
Huizache	Hu-A	4.8 ±2.3	13.1 ± 5.6	35.3 ± 7.3	6.6 ± 1.5	21.3 ± 1.7	28.7 ± 12.2
	Hu-B	8.8 ± 2.5	19.8 ± 3.6	36.6 ±8.7	13.9 ± 2.7	15.3 ± 4.1	29.1 ± 4.3
	Hu-C	9.5 ± 5.1	15.3 ±7.6	33.7 ±16.4	6.8 ±1.4	21.4 ±11.3	21.8 ± 4.0
	Hu-D	5.1 ±1.7	15.8 ±4.5	16.5 ±19.0	7.2 ± 2.3	20.4 ±7.6	29.6 ± 9.0
Agave Bagasse			14.6 ± 8.5			17.4 ± 4	
Comm. Wood			19.8 ± 9.7			25.6 ±19.6	

Table 5. Young Modulus of AAc/AAm hydrogels as a function of CNC type and concentration, and NMBA concentration at 2000 h of swelling.

C_{CNC} (wt. %)		0.1			1		
CNC Type	C_{NMBA} (wt. %)	0.1	0.5	1	0.1	0.5	1
Control		5.8 ±1.22	8.6 ±0.24	19.3±9.5	5.8 ±1.22	8.6 ± .24	19.3±9.5
Huizache	Hu-A	5.7 ± 1.6	10.3±2.3	36 ± 30	9.4 ± 2.9	13.7 ±1.4	18.4 ± 1.3
	Hu-B	5.9 ± 0.2	6.3 ± 4.3	17.2 ± 8.6	7.2 ± 1.7	8.8 ± 1.5	15.7 ± 4.4

 doi:10.20944/preprints202412.0407.v1

Hu-C	3.9 ± 0.6	6.9 ± 0.37	17.8±26.6	4.7 ± 0.6	13.1±16.4	17.7 ± 2.1
Hu-D	5.9 ± 0.7	6.7 ± 2.9	9.0 ± 4.1	8.1 ±1.6	12.3 ± 1.2	15.2 ±5.9
Agave Bagasse		16.1±2.3			23.6 ± 5.8	
Comm. Wood		15.27±3.3			11.0 ± 4.8	

3. Conclusions

Hydrogels with a ratio of acrylic monomers (AAm/AAc) of 50/50 reinforced with CNC obtained from various sources were synthesized using a photosensitive initiator. The increased the N-N methylene bis-acrylamide (NMBA) concentration decreases the swelling capacity. Consequently, the hydrogel presents more resistance to compression, exhibiting a higher value of Young's modulus, this, regardless of the concentration of CNC.

The degree of substitution of sulfate groups in CNCs was determined under various hydrolysis conditions. FTIR also examined the functional groups of the hydrogels. The effect of NMBA is manifested in the band at 1271 cm-1, while a decrease in the normalized area bands (A/A1731) was observed for the wavenumber of 1455 and 2834 cm-1 with the increase of acid groups in the cellulose. This behavior suggests that a higher degree of substitution limits the interaction of the OH groups of cellulose with the reaction system, hindering cross-linking reactions. Consequently, a higher concentration of acid groups on CNC is associated with a lower degree of hydrogel crosslinking, and, therefore, they exhibit higher swelling capacity than those with CNC with lower sulfate groups concentration, resulting in a reduction in mechanical properties.

Nevertheless, this behavior is more complex since the mechanical properties depend more on the synergies between the concentrations of cross-linking agents and CNC as sulfate groups concentration on CNC. At low concentrations of NMBA, CNC improves mechanical properties; However, at high concentrations, these properties deteriorate, suggesting the presence of percolation conditions due to the interaction between NMBA and CNC in the hydrogel. On the other hand, the morphological analysis revealed that the pore size decreases with increasing concentration of NMBA and CNC, and that incorporating CNC generates hydrogels with softer textures. Finally, it was evidenced that the swelling kinetic behavior of hydrogel fit the second order Schott equation for times lower than 500 h, y for more significant times, the swelling behavior is linear, and mechanical properties diminish with swelling degree.

4. Materials and Methods

4.1. Materials

Sulfuric acid (H_2SO_4, 99%), sodium hypochlorite ($NaClO_2$, 97% purity), sodium hydroxide (NaOH, 97% purity), methanol (CH_3OH, 99% purity) and hydrogen peroxide (H_2O_2, 30% purity) from Golden Bell Reagents (Zapopan, Mexico) were used. Acrylamide AAm (CH_2=CHCONH$_2$, 99 %, purity), acrylic acid AAc (CH_2=CHCOOH 99 %, purity), N,N-methilenebisacrylamide NMBA ((CH_2=CHCONH)$_2CH_2$, 99 %, purity), 2,2-dimethoxy-2-phenylacetophenone ($C_6H_5COC(OCH_3)_2C_6H_5$, 99 %, purity), cupriethylenediamine CED ($Cu(H_2NCH_2NH_2)_2(OH)_2$, 1M in H_2O, 97 % purity), and anthraquinone ($C_{14}H_7NAO_5S$, 97 %, purity) were purchased from Sigma-Aldrich (Toluca, México). Sodium thiosulfate ($Na_2S_2O_3$, 0.1 N 96 % purity) was acquired from Karal Reactivos Analíticos (León, México).

4.2. Preparation and Characterization of Soluble Grade Cellulose Pulp

Huizache wood from Tala, Jalisco, Mexico was used. The wood was chipped and dried in the environment for 72 hours, then sifted and classified. The chips used in this work were those retained in mesh 7. The soluble grade pulp was obtained using the method reported by Lopez (2017) [103], which consists of pre-hydrolysis, alkaline cooking, and six bleaching bleaching [15]. For the pre-hydrolysis process, 500 g of chips were mixed with a 0.5% sulfuric acid solution and heated to 160° C for 30 min. The material was then washed and subjected to an alkaline pulping process with a 24% Na_2SO_3/NaOH solution (70/30 w/w ratio) with 0.1% anthraquinone and 20%V methanol [104].

 doi:10.20944/preprints202412.0407.v1

Cooking was carried out in a Jayme digester (Manufacturer: Scientific and Technical Services at the UPC, Barcelona, Spain), with a 5:1 hydromodule, at 170 °C for 150 min. The resulting pulp was washed and purified for subsequent bleaching using the following bleaching sequence: Chlorination-Alkaline extraction-Chlorine dioxide-Hydrogen peroxide-Alkaline extraction-Hydrogen peroxide (C-E1-D-P1-E2-P2) [105].

The resulting Huizache wood pulp was evaluated by measuring various parameters of interest, such as Kappa number (TAPPI T 236 om-22)[106], viscosity (TAPPI T 230 om-19) [107], whiteness (TAPPI T 452 om-18) [108] and α, β and γ-cellulose content (TAPPI T 203 cm-22) [109].

4.3. Obtaining and Characterization of Cellulose Nanocrystals

Before the hydrolysis reaction, the soluble grade cellulose pulp is pulverized by grinding in a knife mill, equipped with a 200 mesh sieve. The CNCs were obtained by acid hydrolysis, using sulfuric acid at different concentrations for various temperatures and treatment times (see Table 6). The cellulose nanocrystal suspensions were centrifuged, dialyzed, filtered, and stored at 4 °C. The average size of the CNCs and the residual load of strong acid groups were determined, in mmol per kg of CNC.

Table 6. Experimental conditions for obtaining nanocrystals.

CNC Source	CNC ID	[H_2SO_4]	T (°C)	t (min)	Filter size (μm)
Huizache	Hu-A	62.5	50	55	1.6
	Hu-B	65	55	65	1.6
	Hu-C	60	55	64	6
	Hu-D	60	55	45	1.6
Agave Bagasse	AB	63.5	44	130	-
Comm. Wood	CW	64	-	-	-

4.3.1. Determination of the Residual Charge in NCC, by Conductance Titration

The conductimetric analysis was performed by placing a conductivity electrode and a pH electrode from a Thermo Scientific Orion Star A215 pH meter (Waltham, MA, USA) inside a three-neck flask. At the same time, a NaOH 0.05 solution was placed in a digital burette. Both devices are connected to a computer to record the volume of added sodium hydroxide and the corresponding pH and conductivity values (mS/Cm). The evaluations are developed in an inert environment with argon to preventCO_2 absorption during the analysis.

4.3.2. Particle Size Distribution by Dynamic Light Scattering (DLS)

A Malvern brand DLS equipment, model Zetasizer Nano S90 (Malvern, Worcestershire, U.K.) was used. Previously, the CNC samples were sonicated in an Elma brand ultrasound bath (Singen, Germany) for 5 min at room temperature. 200 μL of the suspension was taken and diluted by adding 800 μL of deionized water (18 MΩ-cm).

4.3.3. AFM Morphological Analysis

The cellulose nanoparticle samples were diluted to a concentration of 0.2% v/v, these were filtered using a syringe filter of 25 mm diameter and 1.6 μm pore size. The suspensions were then sonicated in an ultrasonic bath at a frequency of 20 KHz for 5 minutes. Finally, 10 μL of the suspensions were deposited on V1 grade mica discs and allowed to dry at room temperature.4.4. Hydrogel synthesis and characterization. The CNCs were analyzed using a Park Systems AFM microscope (Park Systems Corp, Suwon, South Korea). The tapping mode technique was used. Amplitude, height and phase images of 2 x 2 μm and 5 x 5 μm sections of the sample were taken with

 doi:10.20944/preprints202412.0407.v1

a resolution of 512/512 pixels/line. Aluminum-coated silicon microtips model AC160TS-R3 (from Oxford Instruments, Abing-don, UK) were used for image acquisition.

4.3.4. Hydrogel Synthesis

The hydrogels were synthesized via solution polymerization, the monomeric composition AAc/AAm was 50/50 w/w, and the study variables were the concentration of crosslinking agent (C_{NMBA}: 0.1, 0.5 and 1 wt. % as a function of monomeric phase), the concentration of CNC (C_{CNC}: 0.1 and 1 wt. % concerning the monomers), type of CNC, from Huizache (Hu-Hu-B, Hu-C and, Hu-D), Agave bagasse and commercial CNC from wood Table 6). The compositions of the hydrogels with respect to the variables are shown in Table 7:

Table 7. NMBA and CNC concentrations on hydrogels for the different CNC types.

CNC type	[NMBA] (wt. %)	[CNC] (wt. %)
Control Sample	0.1, 0.5 and 1	0
Hu-A	0.1, 0.5 and 1	0.1 and 1
Hu-B	0.1, 0.5 and 1	0.1 and 1
Hu-C	0.1, 0.5 and 1	0.1 and 1
Hu-D	0.1, 0.5 and 1	0.1 and 1
AB	0.5	0.1 and 1
CW	0.5	0.1 and 1

The procedure consisted of mixing 10 g of acrylic acid and 10 g of acrylamide, NMBA 0.1, 0.5, or 1.0 % by weight agree to the monomeric phase was added, samples without CNC (Control) and with CNC 0.1 or 1 wt. % concerning the monomeric phase were prepared. Subsequently, double-distilled water was added to 50 mL of reaction solution, which was placed in refrigeration until reaching 3°C ± 1, finally 1 mL of photoinitiator solution was added (3 g of 2,2-dimethoxy-2-phenylacetophenone, in 100 mL of methanol). The reaction solution was poured into a 0.450 L glass semi-infinite plate reactor, which was contained in an isothermal bath at 3°C. A F15T8-BLB lamp (20W of 127v), Tecno brand (purchased from Electrica Variedades Guadalajara, Jal., Mexico) was placed 20 cm away from the reaction system; the lamp is rich in radiation of 366 nm wavelength. After this time, cylindrical test tubes of 10 mm in diameter and 5 mm in height were stamped. The test tubes were dried and weighed, recording the weight as W_0. Then, polymers were washed by immersing them in double-distilled water and changing the water every 24 hours for a week to eliminate residues of unreacted monomers and polymers not bound to the network. They were then left to dry in an oven at 30 °C for 3 days to obtain xerogels, and were weighed and the weight recorded as Wx. The polymer gel fraction (GF) was calculated as follows:

$$GF = \frac{W_x}{W_0} 100 \qquad (1)$$

where: Wx is the weight of the dry, insoluble polymer (xerogel) after washing with water; and, W_0 is the initial weight of the polymer.

4.3.5. FTIR Spectroscopy

The samples were dried in an oven at 50 °C for 48 hours. The spectra were obtained on a Perkin Elmer FTIR spectrophotometer, model Spectrum GX, (Waltham, MA, USA). 24 scans were taken in the range of 4000 to 400 cm^{-1}.

4.3.6. Swelling Kinetics

The dried samples were weighed and placed in double-distilled water at 25 °C. Five samples were analyzed for each hydrogel composition, and the average of these 5 measurements is reported. The samples were weighed at different hydration times. The absorbent paper was used to remove the excess water from the samples' surfaces. The amount of water absorbed was calculated by the

 doi:10.20944/preprints202412.0407.v1

difference in weight between the weight of the dry sample and the weight of the swollen sample using the following equation:

$$S_w = \frac{W_t - W_0}{W_0} \quad (2)$$

where W_t is the weight of the hydrogel at time t, and W_0 is the weight of the xerogel. The experimental results were fitted agree with the second-order model proposed by Schott [87], which is commonly used to predict swelling in acrylic hydrogels [4,110]:

$$\frac{dS_w}{dt} = k(S_{w,\infty} - S_w)^2 \quad (3)$$

where S_w and $S_{w,\infty}$ are the swellings at time t and at equilibrium, respectively, and K is a system constant.

Integrating equation (3), we obtain:

$$S_w = \frac{kS_{w,\infty}^2 t}{1 + kS_w t} \quad (4)$$

Equation (4) represents second-order kinetics in quadratic form, i.e. the swelling rate at any time is directly proportional to the square of the swelling capacity still available, i.e. the solvent uptake that has not yet occurred before reaching the maximum or equilibrium uptake [110].

4.3.7. Scanning Electron Microscopy (SEM)

The xerogels were hydrated for various hydration times, immersed in liquid nitrogen for 3 min to freeze, and immediately fractured. They were freeze-dried in Labconco (Kansas, MO, USA) equipment for 48 h at a temperature of -47 °C and a vacuum of 70 x 10^{-3} Mbar. The xerogels were then re-coated with Au. The samples were observed in a TESCAN electron microscope, model MIRA 3 LMU from Keyence (Osaka, Japan), using an acceleration voltage of 10 kV.

4.3.8. Rheological Characterization of Hydrogels

The Young's modulus of swollen hydrogels was determined at equilibrium, using cylindrical specimens subjected to compression deformation in an AR G2 rheometer (TA Instruments, New Castle, DE, USA) said deformation was carried out at a constant speed of 8 µm/s, and 25 °C, with a textured geometry of 25 mm diameter. The compressive strength, or capacity of a sample to resist compression loads, is measured by crushing a cylindrical sample according to ASTM-D695-23 [111], where this test sample is placed in a compression instrument, and one of the pistons advances at a constant speed. The maximum compressive strength is equal to the load that causes breakage of the material divided by the minimum cross section, since there are many materials that do not break with compression, the strengths that cause a given deformation are recorded [112]. From the data obtained, (Normal force and displacement or gap) the deformation was obtained according to $\delta=(h_0-h)/h_0$, where h_0 is the height of the hydrogel in **µ**m and h is the distance that the hydrogel is compressed, while the compressive strength in Pa is determined by the ratio of the normal force in N, and the area of the hydrogel in m^2. The Young's modulus corresponds to the slope of the first linear zone ($\delta < 5$ %) of the compressive strength as a function of compression [113].

Author Contributions: Conceptualization, G.C.-E, S.G.-E. and E.R.M.-B.; methodology, AB.N.-H., M.A.G.-S., C.L.-L., S.G.-E., and E.R.M.-B.; software, G.L.-G, S.G.-E., and E.R.M.-B.; validation, AB.N.-H., M.A.G.-S., C.L.-L., S.G.-E., and E.R.M.-B.; formal analysis, J.J.V.-R., J.A. C.-O, S.G.-E., and E.R.M.-B.; investigation, AB.N.-H., M.A.G.-S., C.L.-L., S.G.-E., and E.R.M.-B.; resources, J.F.A.S.M., S.G.-E, and E.R.M.-B; data curation, AB.N.-H., M.A.G.-S., C.L.-L., S.G.-E., and E.R.M.-B.; writing—original draft preparation, S.G.-E., and E.R.M.-B.; writing—review and editing, J.F.A.S.-M, G.C.-E., J.A. C.-O, J.J.V.-R, G.L.-G., S.G.-E., and E.R.M.-B.; visualization, J.A. C.-O, and J.J.V.-R.; supervision, J.F.A.S.M., S.G.E., G.C-E. and E.R.M.-B.; project administration, E.R.M.-B., S.G.-E.; funding acquisition, J.F.A.S.-M.,S.G.-E., and E.R.M.-B. All authors have read and agreed to the published version of the manuscript.

Funding: This research was funded by Secretaría de Educación Pública (SEP) for financially supporting the project "Development and innovation in nanomaterials and nanocomposites, from the International Thematic Network", Call 2015.

Data Availability Statement: The data presented in this study are available on request from the corresponding author.

Conflicts of Interest: The authors declare no conflicts of interest.

References

1. Reddy, N. S.; Rao, K. S. V. K. Polymeric hydrogels : Recent advances in Toxic metal ion removal and anticancer drug delivery applications. *Indian Journal of Advances in Chemical Science* **2016**, 4(2), 214–234.
2. Zhou, C.; Wu, Q. A novel polyacrylamide nanocomposite hydrogel reinforced with natural chitosan nanofibers. *Colloids and Surfaces B: Biointerfaces* **2011**, 84(1), 155–162.
3. Swain, S. K.; Prusty, K. Biomedical applications of acrylic-based nanohydrogels. *Journal of Materials Science* **2018**, 53(4), 2303-2325.
4. Lara-Valencia, V. A.; Dávila-Soto, H.; Moscoso-Sánchez, F. J.; Figueroa-Ochoa, E. B.; Carvajal-Ramos, F.; Fernández-Escamilla, V. V. A.; Soltero-Martinez, J.F.A.; Macias-Balleza, E.R.; Enríquez, S. G. The use of polysaccharides extracted from seed of Persea americana var. Hass on the synthesis of acrylic hydrogels. *Quimica Nova* **2018**, 41, 140-150. https://doi.org/10.21577/0100-4042.20170156
5. De Jong, S. J.; De Smedt, S. C.; Wahls, M. W. C.; Demeester, J.; Kettenes-van Den Bosch, J. J.; Hennink, W. E. Novel self-assembled hydrogels by stereocomplex formation in aqueous solution of enantiomeric lactic acid oligomers grafted to dextran. *Macromolecules* **2000**, 33(10), 3680–3686. https://doi.org/10.1021/ma992067g
6. FAO. Valores y usos de especies importantes de árboles y arbustos en la región sur-sureste de México. Food and Agriculture Organization of the United Nations **2023**. https://www.fao.org/3/j0606s/j0606s0a.htm consultado 06 de septiembre de 2023.
7. Smith, T. P.; Wilson, S. B.; Marble, S. C.; Xu, J. Propagation for commercial production of sweet acacia (*Vachellia farnesiana*): a native plant with ornamental potential. *Native Plants Journal* **2022**, 23(3), 337-348.
8. Xu, J.; Wilson, S. B.; Vendrame, W. A.; Beleski, D. G. Micropropagation of sweet acacia (*Vachellia farnesiana*), an underutilized ornamental tree. *In Vitro Cellular & Developmental Biology-Plant* **2023**, 59(1), 74-82.
9. Ramirez, R. G.; Ledezma-Torres, R. A. Forage utilization from native shrubs *Acacia rigidula* and *Acacia farnesiana* by goats and sheep. *Small Ruminant Research* **1997**, 25(1), 43-50.
10. García-Winder, L. R.; Goñi-Cedeño, S.; Olguin-Lara, P. A.; Díaz-Salgado, G.; Arriaga-Jordan, C. M. Huizache (Acacia farnesiana) whole pods (flesh and seeds) as an alternative feed for sheep in Mexico. *Tropical Animal Health and Production* **2009**, 41, 1615-1621.
11. Delgadillo-Puga, C.; Cuchillo-Hilario, M.; León-Ortiz, L.; Ramírez-Rodríguez, A.; Cabiddu, A.; Navarro-Ocaña, A.; Morales-Romero, A.M.; Medina-Campos, O. N.; Pedraza-Chaverri, J. Goats' feeding supplementation with *Acacia farnesiana* pods and their relationship with milk composition: Fatty acids, polyphenols, and antioxidant activity. *Animals* **2019**, 9(8), 515.
12. Barrientos-Ramírez, L.; Vargas-Radillo, J. J.; Rodríguez-Rivas, A.; Ochoa-Ruíz, H. G.; Navarro-Arzate, F.; Zorrilla, J. Evaluation of characteristics of huizache (*Acacia farnesiana* (L.) Willd.) fruit for potential use in leather tanning or animal feeding. *Madera y bosques* **2012**, 18(3), 23-35.
13. Sankaran, K. V.; Suresh, T. A. Invasive alien plants in the forests of Asia and the Pacific. RAP Publication, Bangkok, Thailand 2013.
14. Khan, I. U.; Haleem, A.; Khan, A. U. Non-edible plant seeds of *Acacia farnesiana* as a new and effective source for biofuel production. *RSC advances* **2022**, 12(33), 21223-21234.
15. Ramírez-Casillas, R.; López-López, M.C.; Becerra-Aguilar, B.; Dávalos-Olivares, F.; Satyanarayana, KG. Obtaining dissolving grade cellulose from the huizache (Acacia farnesiana L. Willd.) plant. *BioRecursos* **2019**, 14 (2), 3301-3318.
16. Ramírez-Casillas, R.; López-López, M.; Becerra-Aguilar, B.; Dávalos-Olivares, F.; Satyanarayana, K. G. Preparation and characterization of cellulose nanocrystals using soluble grade cellulose from acid hydrolysis of Huizache (*Acacia farnesiana* L. Willd.). *BioResources* **2019**, 14(2), 3319-3338
17. AL-Tameemi, A. R.; Al-Edany, T. Y.; Attaha, A. H. Phytoremediation of crude oil contaminated soil by *Acacia farnesiana* l. willd. and spraying glutathione. *University of Thi-Qar Journal of Science* **2021**, 8(1), 59-66.
18. Jiménez M., E.; Prieto G., F.; Prieto M., J.; Acevedo S., O. A.; Rodríguez L., R.; Otazo S., E. M. Utilization of Waste Agaves: Potential for Obtaining Cellulose Pulp. *Ciência e Técnica Vitivinícola* **2014**, 29 (11),138–152
19. Berglund, L.; Noël, M.; Aitomäki, Y.; Öman, T.; Oksman, K. Production potential of cellulose nanofibers from industrial residues: Efficiency and nanofiber characteristics. *Industrial Crops and Products* **2016**, 92, 84-92.
20. Nechyporchuk, O.; Belgacem, M. N.; Bras, J. Production of cellulose nanofibrils: A review of recent advances. *Industrial Crops and Products* **2016**, 93, 2-25.

21. Reiniati, I.; Hrymak, A. N.; Margaritis, A. Recent developments in the production and applications of bacterial cellulose fibers and nanocrystals. *Critical reviews in biotechnology* **2017**, 37(4), 510-524.
22. Trache, D.; Hussin, M. H.; Haafiz, M. M.; Thakur, V. K. Recent progress in cellulose nanocrystals: sources and production. *Nanoscale* **2017**, 9(5), 1763-1786.
23. Rånby, B. G.; Banderet, A.; Sillén, L. G. Aqueous Colloidal Solutions of Cellulose Micelles. *Acta Chemica Scandinavica* **1949**, 3, 649-650.
24. Rånby, B. G. Fibrous macromolecular systems. Cellulose and muscle. The colloidal properties of cellulose micelles. *Discuss. Faraday Soc.* **1951**, 11(0), 158–164. doi:10.1039/df9511100158
25. Habibi, Y.; Lucian A. L,; Rojas J. O. Cellulose nanocrystals: chemistry, self-assembly, and applications. *Chemical reviews* **2010**, 110.6, 3479-3500.
26. Moon, R. J.; Martini, A.; Nairn, J.; Simonsen, J.; Youngblood, J. Cellulose nanomaterials review: structure, properties and nanocomposites. *Chemical Society Reviews* **2011**, 40.7, 3941-3994.
27. Fachri, R.; Rizal, S.; Huzni, S.; Ikramullah, I.; Aprilia, S. Production of Cellulose Nanocrystal (CNC) Combine with Silane Treatment from Pennisetum Purpureum via Acid Hydrolysis. *In International Conference on Experimental and Computational Mechanics in Engineering* **2022**, 535-543. Singapore: Springer Nature Singapore.
28. Chen, L.; Wang, Q.; Hirth, K.; Baez, C.; Agarwal, U. P.; Zhu, J. Y. Tailoring the yield and characteristics of wood cellulose nanocrystals (CNC) using concentrated acid hydrolysis. *Cellulose* **2015**, 22, 1753-1762.
29. Sun, B.; Zhang, M.; Hou, Q.; Liu, R.; Wu, T.; Si, C. Further characterization of cellulose nanocrystal (CNC) preparation from sulfuric acid hydrolysis of cotton fibers. *Cellulose* **2016**, 23, 439-450.
30. Gallardo-Sánchez, M. A., Díaz-Vidal, T., Navarro-Hermosillo, A. B., Figueroa-Ochoa, E. B., Ramírez Casillas, R., Anzaldo Hernández, J., Rosales-Rivera, L.C.; Soltero-Martinez, J.F.A.; García-Enriquez S.; Macías-Balleza, E. R. Optimization of the obtaining of cellulose nanocrystals from *Agave equilana* weber var. Azul Bagasse by acid hydrolysis. *Nanomaterials* **2021**, 11(2), 520.
31. Wang, R.; Chen, L.; Zhu, J. Y.; Yang, R. Tailored and integrated production of carboxylated cellulose nanocrystals (CNC) with nanofibrils (CNF) through maleic acid hydrolysis. *ChemNanoMat* **2017**, 3(5), 328-335.
32. Hamad, W. Y. Cellulose nanocrystals: properties, production and applications. John Wiley & Sons. 2017.
33. Fajardo, A. R.; Pereira, A. G.; Muniz, E. C. Hydrogels Nanocomposites Based on Crystals, Whiskers and Fibrils Derived from Biopolymers. In: Thakur, V., Thakur, M. (eds) Eco-friendly Polymer Nanocomposites. Advanced Structured Materials, vol 74. Springer, New Delhi. 2015. https://doi.org/10.1007/978-81-322-2473-0_2
34. Zhou, C.; Wu, Q.; Yue, Y.; Zhang, Q. Application of rod-shaped cellulose nanocrystals in polyacrylamide hydrogels. *Journal of Colloid and Interface Science* **2011**, 353(1), 116–123. https://doi.org/10.1016/j.jcis.2010.09.035
35. Yang, J.; Han, C. R.; Xu, F.; Sun, R. C. Simple approach to reinforce hydrogels with cellulose nanocrystals. *Nanoscale* **2014**, 6(11), 5934-5943.
36. Du, H.; Liu, W.; Zhang, M.; Si, C.; Zhang, X.; Li, B. Cellulose nanocrystals and cellulose nanofibrils based hydrogels for biomedical applications. *Carbohydrate polymers* **2019**, 209, 130-144. https://doi.org/10.1016/j.carbpol.2019.01.020
37. Abitbol, T.; Johnstone, T.; Quinn, T. M.; Gray, D. G. Reinforcement with cellulose nanocrystals of poly (vinyl alcohol) hydrogels prepared by cyclic freezing and thawing. *Soft Matter* **2011**, 7(6), 2373-2379.
38. Song, K.; Zhu, W.; Li, X.; Yu, Z. A novel mechanical robust, self-healing and shape memory hydrogel based on PVA reinforced by cellulose nanocrystal. *Materials Letters* **2020**, 260, 126884.
39. Wang, Y.; Liu, S.; Wang, Q.; Fu, X.; Fatehi, P. Performance of polyvinyl alcohol hydrogel reinforced with lignin-containing cellulose nanocrystals. *Cellulose* **2020**, 27, 8725-8743.
40. Wang, H.; Li, Z.; Zuo, M.; Zeng, X.; Tang, X.; Sun, Y.; Lin, L. Stretchable, freezing-tolerant conductive hydrogel for wearable electronics reinforced by cellulose nanocrystals toward multiple hydrogen bonding. *Carbohydrate Polymers* **2022**, 280, 119018.
41. Zhang, X.; Huang, J.; Chang, P. R.; Li, J.; Chen, Y.; Wang, D.; Yu, J.; Chen, J. Structure and properties of polysaccharide nanocrystal-doped supramolecular hydrogels based on cyclodextrin inclusion. *Polymer* **2010**, 51(19), 4398-4407. https://doi.org/10.1016/j.polymer.2010.07.025
42. Yang, J.; Han, C. R.; Duan, J. F.; Xu, F.; Sun, R. C. Mechanical and viscoelastic properties of cellulose nanocrystals reinforced poly (ethylene glycol) nanocomposite hydrogels. *ACS applied materials & interfaces* **2013**, 5(8), 3199-3207.
43. Cha, R.; He, Z.; Ni, Y. Preparation and characterization of thermal/pH-sensitive hydrogel from carboxylated nanocrystalline cellulose. *Carbohydrate Polymers* **2012**, 88(2), 713-718.
44. Zubik, K.; Singhsa, P.; Wang, Y.; Manuspiya, H.; Narain, R. Thermo-Responsive Poly(N-Isopropylacrylamide)-Cellulose Nanocrystals Hybrid Hydrogels for Wound Dressing. *Polymers* **2017**, 9, 119. https://doi.org/10.3390/polym9040119

 doi:10.20944/preprints202412.0407.v1

45. Wang, J.; Cheng, Q.; Feng, S.; Zhang, L.; Chang, C. Shear-aligned tunicate-cellulose-nanocrystal-reinforced hydrogels with mechano-thermo-chromic properties. *Journal of Materials Chemistry C* **2021**, 9(19), 6344-6350.
46. Yang, J.; Han, C. Mechanically viscoelastic properties of cellulose nanocrystals skeleton reinforced hierarchical composite hydrogels. *ACS applied materials & interfaces* **2016**, 8(38), 25621-25630.
47. Voronova, M. I.; Surov, O. V.; Afineevskii, A. V.; Zakharov, A. G. Properties of polyacrylamide composites reinforced by cellulose nanocrystals. *Heliyon* **2020**, 6(11).
48. Ortega, A.; Valencia, S.; Rivera, E.; Segura, T.; Burillo, G. Reinforcement of Acrylamide Hydrogels with Cellulose Nanocrystals Using Gamma Radiation for Antibiotic Drug Delivery. Gels 2023, 9, 602. https://doi.org/10.3390/gels9080602
49. Jiménez-Amezcua, R. M., Villanueva-Silva, R. J., Muñoz-García, R. O., Macias-Balleza, E. R., Sydenstricker Flores-Sahagun, M. T., Lomelí-Ramírez, M. G., Torres-Rendón, J. G.; Garcia-Enriquez, S. Preparation of Agave tequilana Weber nanocrystalline cellulose and its use as reinforcement for acrylic hydrogels. *BioResources* **2021**, 16(2), 2731
50. Wan Ishak, W. H.; Yong Jia, O.; Ahmad, I. pH-responsive gamma-irradiated poly (acrylic acid)-cellulose-nanocrystal-reinforced hydrogels. *Polymers* **2020**, 12(9), 1932.
51. El Idrissi, A.; El Gharrak, A.; Achagri, G.; Essamlali, Y.; Amadine, O.; Akil, A.; Sair, S.; Zahouily, M. Synthesis of urea-containing sodium alginate-g-poly (acrylic acid-co-acrylamide) superabsorbent-fertilizer hydrogel reinforced with carboxylated cellulose nanocrystals for efficient water and nitrogen utilization. *Journal of Environmental Chemical Engineering* **2022**, 10(5), 108282.
52. Al-Gorair, A. S; Sayed, A.; Mahmoud, G. A. Engineered superabsorbent nanocomposite reinforced with cellulose nanocrystals for remediation of basic dyes: isotherm, kinetic, and thermodynamic studies. *Polymers* **2022**, 14(3), 567.
53. Dai, Q.; Kadla, J. F. Effect of nanofillers on carboxymethyl cellulose/hydroxyethyl cellulose hydrogels. *Journal of applied polymer science* **2009**, 114(3), 1664-1669.
54. Ishak, W. H. W.; Rosli, N. A.; Ahmad, I.; Ramli, S.; Amin, M. C. I. M. Drug delivery and in vitro biocompatibility studies of gelatin-nanocellulose smart hydrogels cross-linked with gamma radiation. *Journal of Materials Research and Technology* **2021**, 15, 7145-7157.
55. do Nascimento, D. M.; Nunes, Y. L.; Feitosa, J. P.; Dufresne, A.; Rosa, M. D. F. Cellulose nanocrystals-reinforced core-shell hydrogels for sustained release of fertilizer and water retention. *International Journal of Biological Macromolecules* **2022**, 216, 24-31.
56. Tang, J.; Javaid, M. U.; Pan, C.; Yu, G.; Berry, R. M.; Tam, K. C. Self-healing stimuli-responsive cellulose nanocrystal hydrogels. *Carbohydrate polymers* **2020**, 229, 115486.
57. Yan, H.; Huang, D.; Chen, X.; Liu, H.; Feng, Y.; Zhao, Z.; Zhang, X.; Lin, Q. A novel and homogeneous scaffold material: preparation and evaluation of alginate/bacterial cellulose nanocrystals/collagen composite hydrogel for tissue engineering. *Polymer Bulletin* **2018**, 75, 985-1000.
58. Soleimani, S.; Heydari, A.; Fattahi, M.; Motamedisade, A. Calcium alginate hydrogels reinforced with cellulose nanocrystals for methylene blue adsorption: Synthesis, characterization, and modelling. *Industrial Crops and Products* **2023**, 192, 115999.
59. Soleimani, S.; Heydari, A.; Fattahi, M. Swelling prediction of calcium alginate/cellulose nanocrystal hydrogels using response surface methodology and artificial neural network. *Industrial Crops and Products* **2023**, 192, 116094.
60. Olad, A.; Doustdar, F.; Gharekhani, H. Fabrication and characterization of a starch-based superabsorbent hydrogel composite reinforced with cellulose nanocrystals from potato peel waste. *Colloids and Surfaces A: Physicochemical and Engineering Aspects* **2020**, 601, 124962.
61. Catori, D. M.; Fragal, E. H.; Messias, I.; Garcia, F. P.; Nakamura, C. V.; Rubira, A. F. Development of composite hydrogel based on hydroxyapatite mineralization over pectin reinforced with cellulose nanocrystal. *International Journal of Biological Macromolecules* **2021**, 167, 726-735.
62. Liu, D.; Dong, X.; Han, B.; Huang, H.; Qi, M. Cellulose nanocrystal/collagen hydrogels reinforced by anisotropic structure: Shear viscoelasticity and related strengthening mechanism. *Composites Communications* **2020**, 21, 100374.
63. Torabizadeh, F.; Fadaie, M.; Mirzaei, E.; Sadeghi, S.; Nejabat, G. R. Tailoring structural properties, mechanical behavior and cellular performance of collagen hydrogel through incorporation of cellulose nanofibrils and cellulose nanocrystals: A comparative study. *International Journal of Biological Macromolecules* **2022**, 219, 438-451
64. Patel, D.K.; Ganguly, K.; Hexiu, J.; Dutta, S.D.; Patil, T.V.; Lim, K.T. Functionalized chitosan/spherical nanocellulose-based hydrogel with superior antibacterial efficiency for wound healing. *Carbohydrate Polymers* **2022**, 284, 119202.
65. Maturavongsadit, P.; Paravyan, G.; Shrivastava, R.; Benhabbour, S. R. Thermo-/pH-responsive chitosan-cellulose nanocrystals based hydrogel with tunable mechanical properties for tissue regeneration applications. *Materialia* **2020**, 12, 100681.

66. López L., M.C. Estudio biométrico y químico de la planta silvestre huizache (Acacia farnesiana) y su influencia en la calidad de fibra celulósica. Bachelor's thesis in Biology. University of Guadalajara 2012.
67. MacLeod, J. M.; Fleming, B. I.; Kubes, G. J.; Bolker, H. I. The strengths of kraft-AQ [anthraquinone] and soda-AQ pulps: bleachable-grade pulps [of softwoods]. TAPPI ,Technical Association of the Pulp and Paper Industry, 1980, USA.
68. Sixta, H.; Schild, G. A new generation kraft process. *Lenzinger Berichte* **2009**, 87(1), 26-37.
69. Behin, J.; Mikaniki, F.; Fadaei, Z. Dissolving pulp (alpha-cellulose) from corn stalk by kraft process. *Iranian Journal of Chemical* Engineering **2008**, 5 (3): 14-28
70. Sixta, H. Handbook of pulp, Wiley-VCH, Verlag GMbH and Co, KGaA, Weinheim, 2006.
71. Chen, C.; Duan, C.; Li, J.; Liu, Y.; Ma, X.; Zheng, L.; Stavik, J.; Ni, Y. Cellulose (dissolving pulp) manufacturing processes and properties: A mini-review. *BioResources* **2016**, 11(2), 5553-5564.
72. Wertz, J.L.; Bédué, O.; Mercier, J.P. Swelling and Dissolution of Cellulose; in Cellulose Science and Technology. EPFLPress, Lausana, Suiza, **2010**; pag. 62.
73. Oberlerchner, J. T.; Rosenau, T.; Potthast, A. Overview of methods for the direct molar mass determination of cellulose. *Molecules* **2015**, 20(6), 10313-10341.
74. Beck-Candanedo S.; Roman M.; Gray D.G.Effect of reaction conditions on the properties and behavior of wood cellulose nanocrystal suspensions. *Biomacromolecules* **2005**, 6:1048-1054
75. Lima M. M. D.; Borsali R. Rodlike cellulose microcrystals: structure, properties, and applications. *Macromol. Rapid Commun* **2004**. 25:771–787.
76. Schulz B. P.C., Leslie A., A.; Rubio, E. Espectroscopia de infrarrojo. Ed. University of Guadalajara, Mexico,1989.
77. Katsumoto, Y., Tanaka, T., & Ozaki, Y. (2005). Molecular Interpretation for the Solvation of Poly (acrylamide) s. I. Solvent-Dependent Changes in the CO Stretching Band Region of Poly (N, N-dialkylacrylamide) s. The Journal of Physical Chemistry B, 109(44), 20690-20696. https://doi.org/10.1021/jp052263r
78. Murugan, R.; Mohan, S.; Bigotto, A. FTIR and polarised Raman spectra of acrylamide and polyacrylamide. *Journal of the Korean Physical Society* **1998**, 32(4), 505.
79. Hirose, K.; Ihashi, Y.; Taguchi, S.; Yoshizawa, M. Infrared Spectra of Polymethylenebisacrylamide. *Nippon Kagaku Kaishi* **1966**, 69, 240-244.
80. Magalhães, A. S. G.; Almeida N., M. P.; Bezerra, M. N.; Ricardo, N. M.; Feitosa, J. Application of FTIR in the determination of acrylate content in poly (sodium acrylate-co-acrylamide) superabsorbent hydrogels. *Química Nova* **2012**, 35, 1464-1467.
81. Yu, H.Y.; Qin, Z.Y.; Liu, L.; Yang, X.G.; Zhou, Y.; Yao, J.M. Comparison of the reinforcing effects for cellulose nanocrystals obtained by sulfuric and hydrochloric acid hydrolysis on the mechanical and thermal properties of bacterial polyester. *Compos. Sci. Technol.* **2013**, 87, 22–28.
82. Anwar, B.; Bundjali, B.; Arcana, I.M. Isolation of Cellulose Nanocrystals from Bacterial Cellulose Produced from Pineapple Peel Waste Juice as Culture Medium. *Procedia Chem.* **2015**, 16, 279–284.
83. Contreras, H.J.; Trujillo, H.A.; Arias, G.; Pérez, J.; Delgado, E. Espectroscopia Atr-Ftir De Celulosa: Aspecto Instrumental Y Tratamiento Matemático De Espectros. *e-Gnosis* **2010**, 8, 1–13.
84. Orozco-Guareño, E.; Hernández, S. L.; Gómez-Salazar, S.; Mendizábal, E.; Katime, I. Estudio del hinchamiento de hidrogeles acrílicos terpoliméricos en agua y en soluciones acuosas de ión plumboso. *Revista Mexicana de Ingeniería Química* **2011**, 10(3), 465-470.
85. Nesrinne, S.; Djamel, A. Synthesis, characterization and rheological behavior of pH sensitive poly (acrylamide-co-acrylic acid) hydrogels. *Arabian Journal of Chemistry* **2017**, 10(4), 539-547.
86. Wen, Y.; Zhu, X.; Gauthier, D.E.; An, X.; Cheng, D.; Ni, Y.; Yin, L. Development of poly (acrylic acid)/nanofibrillated cellulose superabsorbent composites by ultraviolet light induced polymerization. *Cellulose* **2015**, 22, 2499–2506. https://doi.org/10.1007/s10570-015-0639-6
87. Schott, H. Swelling kinetics of polymers. *Journal of Macromolecular Sciencie, Part B* **1992**, 31(1), 1–9. Retrieved from http://www.tandfonline.com/doi/pdf/10.1080/00222349208215453?needAccess=true
88. Zhou, C.; Wu, Q.; Yue, Y.; Zhang, Q. Application of rod-shaped cellulose nanocrystals in polyacrylamide hydrogels. *Journal of Colloid and Interface Science* **2011**, 353(1), 116–123. https://doi.org/10.1016/j.jcis.2010.09.035
89. Lim, L.; Rosli, N. A.; Ahmad, I.; Mat, A.; Amin, M. Synthesis and swelling behavior of pH-sensitive semi-IPN superabsorbent hydrogels based on poly(acrylic acid) reinforced with cellulose nanocrystals. *Nanomaterials* **2017**, 7(12), 399–412.
90. Iliasov, L.; Shibaev, A.; Panova, I.; Kushchev, P.; Philippova, O.; Yaroslavov, A. Weakly Cross-Linked Anionic Copolymers: Kinetics of Swelling and Water-Retaining Properties of Hydrogels. *Polymers* **2023**, 15(15), 3244.
91. Kumari, R.; Shekhar, S. Effect of Crosslinking on Thermodynamics Interactions and Network Parameters of Terpolymeric Hydrogels. *Journal of Macromolecular Science, Part B* **2023**, 62(12), 689-717.

 doi:10.20944/preprints202412.0407.v1

92. Scallan, A. M. The effect of acidic groups on the swelling of pulps: a review. *Tappi journal* **1983**, 66(11), 73-75.
93. Burke, N. I. U.S. Patent No. 4,233,329. Washington, DC: U.S. Patent and Trademark Office, 1980.
94. Işık, B. Swelling Behavior and Determination of diffusion characteristics of acrylamide–acrylic acid hydrogels. *Journal of Applied Polymer Science* **2003**, 91(2), 1289–1293.
95. Li, Y.; Dong, X.; Yao, L.; Wang, Y.; Wang, L.; Jiang, Z.; Qiu, D. Preparation and Characterization of Nanocomposite Hydrogels Based on Self-Assembling Collagen and Cellulose Nanocrystals. *Polymers* **2023**, 15(5), 1308. https://doi.org/10.3390/polym15051308
96. Wong, R. S. H.; Ashton, M.; Dodou, K. Effect of crosslinking agent concentration on the properties of unmedicated hydrogels. *Pharmaceutics* **2015**, 7(3), 305-319.
97. Xiong, Y.; Zhang, X.; Liu, M. Z. Effect of crosslinker type on the properties of surface-crosslinked poly (sodium acrylate) superabsorbents. *Advanced Materials Research* **2014**, 936, 89-94.
98. Anseth, K. S.; Bowman, C. N.; Brannon-Peppas, L. Mechanical properties of hydrogels and their experimental determination. *Biomaterials* **1996**, 17(17), 1647-1657.
99. Noteborn, W. E.; Zwagerman, D. N.; Talens, V. S.; Maity, C.; van der Mee, L.; Poolman, J. M.; Mytnyk S.; van Esch, J.H.; Kros, A.; Eelkema, R.; Kieltyka, R. E. Crosslinker-Induced Effects on the Gelation Pathway of a Low Molecular Weight Hydrogel. *Advanced Materials* **2017**, 29(12), 1603769.
100. Davis, T. P.; Huglin, M. B. Effect of crosslinker on properties of copolymeric N-vinyl-2-pyrrolidone/methyl methacrylate hydrogels and organogels. *Die Makromolekulare Chemie* **1990**, 191(2), 331-343.
101. Tanpichai, S.; Oksman, K. Cross-linked nanocomposite hydrogels based on cellulose nanocrystals and PVA: Mechanical properties and creep recovery. *Composites Part A: Applied Science and Manufacturing* **2016**, 88, 226-233.
102. Keyvani, P.; Nyamayaro, K.; Mehrkhodavandi, P.; Hatzikiriakos, S. G. Cationic and anionic cellulose nanocrystalline (CNC) hydrogels: A rheological study. *Physics of Fluids* **2021**, 33(4).
103. Lopez L., M.C. Obtención y caracterización de nanocristales de celulosa, a partir de Huizache, producidos mediante diversas condiciones de hidrolisis acida controlada. Master's thesis. University of Guadalajara, 2017.
104. Morales R., J. P. Estudios sobre el comportamiento de la madera de huizache (Acacia farnesiana) en procesos de pulpeo, enfocados hacia la producción de α-celulosa para derivados. Chemical Engineering Masters thesis, . University of Guadalajara, Mexico, 2013.
105. Muñoz R., M. G. Blanqueo de pulpas de huizache (Acacia farnesiana) para la obtención de α-celulosa para derivados. Chemical Engineering Masters thesis. University of Guadalajara, Mexico, 2013.
106. TAPPI T236 om-22. Kappa Number of Pulp. STANDARD by Technical Association of the Pulp and Paper Industry, Tappi Press, Atlanta, GA, USA, 2022.
107. TAPPI T230 om-19 Viscosity of Pulp (Capillary Viscometer Method). STANDARD by Technical Association of the Pulp and Paper Industry, Tappi Press, Atlanta, GA, USA, 2019.
108. TAPPI T252 om-18. Brightness of pulp, paper, and paperboard (directional reflectance at 457 nm). STANDARD by Technical Association of the Pulp and Paper Industry, TAPPI Press, Atlanta, GA, USA.2018.
109. TAPPI T 203 cm-22. Alpha-, Beta- and Gamma-Cellulose in Pulp. STANDARD by Technical Association of the Pulp and Paper Industry, Tappi Press, Atlanta, GA, USA, 2022.
110. Katime, I.; Velada, J.L.; Novoa, R.; Díaz de Apodaca, E.; Puig, J.; Mendizabal, E. Swelling Kinetics of Poly (acrylamide)/Poly (mono-n-alkyl itaconates) Hydrogels. *Polym. Int.* **1996**, 40, 281–286.
111. ASTM International. D695-23. Standard Test Method for Compressive Properties of Rigid Plastics; ASTM International: West Conshohocken, PA, USA, 2023.
112. Raimond, B. S.; Carraher, C. E. Introducción a la química de los polímeros. Reverté SA, 1995.
113. Rodriguez, F.; Cohen, F.; Ober C. K.; Archer, L. Principles of polymer systems. CRC Press, 2003.